Biogeosciences, 23, 1859–1880, 2026
https://doi.org/10.5194/bg-23-1859-2026
© Author(s) 2026. This work is distributed under
the Creative Commons Attribution 4.0 License.

Biogeosciences
Open Access
EGU

Research article

On the role of light and vertical mixing in shaping Southwestern Atlantic shelf blooms

Ana I. Dogliotti[1,2], Reinaldo A. Maenza[3], Moira Luz Clara[3,4], Vivian A. Lutz[3,4], and Robert Frouin[5]

[1]Instituto de Astronomía y Física del Espacio (IAFE), Consejo Nacional de Investigaciones Científicas y Técnicas (CONICET) – Universidad de Buenos Aires (UBA), Ciudad Autónoma de Buenos Aires, C1428ZAA, Argentina
[2]Instituto Franco-Argentino para el Estudio del Clima y sus Impactos (UMI-IFAECI, CNRS CONICET-UBA), Buenos Aires, C1428EGA, Argentina
[3]Instituto Nacional de Investigación y Desarrollo Pesquero (INIDEP), Paseo Victoria Ocampo No. 1, Escollera Norte, Mar del Plata, B7602HSA, Argentina
[4]Instituto de Investigaciones Marinas y Costeras (IIMYC), Facultad de Ciencias Exactas y Naturales, Universidad Nacional de Mar del Plata (UNMDP), Consejo Nacional de Investigaciones Científicas y Técnicas (CONICET), CC 1260, Mar del Plata, B7600, Argentina
[5]Scripps Institution of Oceanography, University of California, San Diego, La Jolla, California 92037, United States

Correspondence: Robert Frouin (rfrouin@ucsd.edu)

Received: 30 April 2025 – Discussion started: 26 June 2025
Revised: 22 December 2025 – Accepted: 30 December 2025 – Published: 11 March 2026

Abstract. The influence of light availability and mixed layer depth (MLD) on phytoplankton bloom dynamics was examined across the Argentine Continental Shelf in the Southwest Atlantic Ocean (SWAO). Using satellite-derived chlorophyll-*a* concentration (Chl-*a*), photosynthetically available radiation (PAR), and euphotic depth (Z_{eu}, defined as the depth at which the irradiance is 1 % of its PAR value at surface) data, together with reanalysis products for MLD and wind fields, we analyzed the spatial and temporal variability of key phenological parameters computed from the Chl-*a* time series, including bloom initiation, peak timing, and bloom intensity, over the 1998–2019 period. Distinct mean spatial distribution patterns in bloom dynamics were observed. In the Central Shelf (CS), blooms typically initiate (May–August) and peak (September–November) relatively early which correlated with shallow MLDs and increasing light, while coastal areas showed even earlier initiation (April) due to highly variable environmental conditions. In turn, the Patagonian Shelf (PS) experienced delayed initiation (September onwards) and peaks (December–January) probably due to deeper MLDs as result of the colder Subantarctic waters. Bloom intensity also exhibited spatial variability, with the highest values observed in the southern PS and regions influenced by frontal systems, where nutrient-rich upwelling and favorable light conditions enhanced phytoplankton growth. Statistical modeling revealed that light penetration (Z_{eu}) and its interplay with vertical mixing (Z_{eu} : MLD ratio) were the strongest predictors of bloom anomalies at most sites. However, the predictive power of these relationships varied in regions influenced by local processes, like tidal mixing or frontal zones. Predictive models need to be integrated with regional oceanographic features to improve assessments of bloom phenology and primary production in such highly variable shelf ecosystems.

1 Introduction

The Earth's oceans are dynamic ecosystems influenced by many factors, including solar irradiance, nutrient availability, trophic interactions, and physical processes such as vertical mixing. Some of these processes can be encompassed by the evaluation of the mixed layer depth (MLD), which represents the portion of the upper ocean most directly affected by turbulent mixing, interacting with the atmosphere. The degree of vertical mixing within this layer largely determines the exposure of most phytoplankton, except for taxa with sufficient vertical motility, to different nutrient and

light conditions. Hence, the light field and the MLD play crucial roles in shaping the distribution and abundance of phytoplankton, the primary producers at the base of marine food webs (Cullen, 2015; Margalef, 1978; Platt et al., 2005; Richardson and Bendtsen, 2019; Sverdrup, 1953). Understanding the effects of these variables is essential for predicting changes in marine ecosystems. One of the key drivers is the alteration of wind patterns, which modulate the mixed-layer depth through their influence on vertical mixing. Additionally, changes in cloud cover affect the amount of solar radiation reaching the ocean surface, directly influencing primary production. These shifts in environmental conditions have profound implications for phytoplankton distribution and abundance, with cascading effects on marine trophic webs and the global carbon cycle (Behrenfeld et al., 2006; Boyd and Doney, 2002; Falkowski et al., 1998).

The light field – through the effect of both incident irradiance in the photosynthetically available radiation (hereafter to as PAR), which determines the energy available for photosynthesis, and the light penetration into the water column, represented by the euphotic zone depth (Z_{eu}) – governs the vertical extent of the upper ocean where light conditions are generally favorable for phytoplankton growth (Behrenfeld and Falkowski, 1997; Platt, 1986). While Z_{eu} is conventionally defined as the depth receiving 1 % of surface PAR and is widely used as an operational metric of light penetration, phytoplankton can photosynthesize and, under certain conditions, grow at lower light levels. Nevertheless, light availability is typically more favorable above this threshold, particularly when considered in combination with vertical mixing and mixed-layer depth. Nutrient availability, particularly nitrogen, phosphorus, and iron, is another critical factor limiting phytoplankton growth in many regions of the ocean (e.g., Moore et al., 2013).

Historically, the understanding of phytoplankton dynamics has been framed by conceptual models such as those proposed by Sverdrup (1953) and Margalef (1978). These models provide qualitative explanations for the mechanisms driving phytoplankton blooms, emphasizing the role of physical processes, like the stability/vertical mixing of the water column, in modulating light and nutrient availability. However, while these conceptual frameworks offer valuable insights, there is a need to develop a way to predict the response of phytoplankton communities to changing environmental conditions.

Recent studies have sought to bridge this gap by incorporating quantitative approaches to assess the relative importance of light (PAR and Z_{eu}) and MLD in determining the timing and intensity of phytoplankton blooms using surface satellite-derived Chl-*a*. While surface chlorophyll does not capture the full, vertically integrated phytoplankton biomass and may miss subsurface maxima, it provides a consistent and widely used proxy for large-scale and long-term analyses of bloom phenology. For instance, Siegel et al. (2002) examined the relationship between phytoplankton bloom dynamics and Sverdrup's Critical Depth Hypothesis in the North Atlantic. They analyzed satellite-derived data and in situ data (reanalysis) to investigate the timing and intensity of the spring phytoplankton bloom in relation to water column stability and light availability, providing evidence supporting Sverdrup's hypothesis. Henson et al. (2009), using satellite chlorophyll and a set of modeled variables, investigated decadal variability in North Atlantic phytoplankton blooms, identifying a strong relationship between changes in MLD, due to shifts in the North Atlantic Oscillation index, and the timing of bloom events, with shallower MLDs coinciding with earlier blooms. This study highlighted the complex interplay between physical processes and biological responses in shaping phytoplankton dynamics on decadal time scales. Platt et al. (2009) investigated the phenology of phytoplankton blooms using remote sensing data. They identified distinct patterns in bloom timing and intensity, correlating with environmental factors like light availability and nutrient concentrations. This research established ecosystem indicators based on bloom dynamics, demonstrating the utility of remote sensing in monitoring and understanding phytoplankton ecology. Marinov et al. (2010) modeled the response of ocean phytoplankton community structure to climate change factors over the 21st century. Their model's results suggested that nutrient availability, temperature, and light significantly influence phytoplankton distribution, i.e., nutrient limitation reduced productivity in certain regions, while warmer temperatures favored specific phytoplankton types. Additionally, changes in light availability, influenced by factors like cloud cover, impacted phytoplankton growth especially at high latitudes, with interactions between these factors contributing to spatial and temporal variability in phytoplankton abundance and composition. Moreover, studies using remote sensing data in the Arctic waters found that sea surface temperature, cloud fraction, wind stress, and sea-ice concentration modulated the bloom initiation, duration and amplitude (Marchese et al., 2017) and that latitude and seasonal changes in sea surface temperature and MLD could influence double bloom occurrences (Zhao et al., 2022). Together, these studies have shed light on the intricate interplay between environmental forces and phytoplankton responses in some oceanic regions, providing insights into the mechanisms driving phytoplankton blooms and their implications for marine habitats and chemical cycling.

The Argentine Sea is characterized by a dynamic oceanographic regime, influenced by the interaction of multiple water masses and complex bathymetric features (Piola and Matano, 2001; Piola et al., 2018). Here, the initiation and development of phytoplankton blooms are highly variable, probably influenced by a combination of physical and biological factors, making it an ideal region for studying the effects of light and MLD on phytoplankton bloom development. Observational studies in the region have highlighted the role of ocean dynamics, such as coastal upwelling events and frontal systems, in driving nutrient enrichment and pro-

moting phytoplankton growth (reviewed in Acha et al., 2004; Carreto et al., 2007). Furthermore, satellite remote sensing data, especially chlorophyll-*a* (Chl-*a*), have provided important information on the seasonal variability and phenological parameters characterizing phytoplankton biomass in the Argentine Sea, revealing distinct patterns of bloom initiation and propagation (Andreo et al., 2016; Delgado et al., 2023). The use of satellite Chl-*a* may sometimes be biased, since the relationship between Chl-*a* and carbon (a closer measure of biomass) in phytoplankton is subject to variability due to species composition and photoacclimation (Cullen, 1985; Geider, 1987; Sathyendranath et al., 2009). Nevertheless, the aim of the present study is not to quantify absolute biomass or productivity, rather analyzing the spatiotemporal variability of bloom intensity and timing based on Chl-*a* patterns; and satellite Chl-*a* has proven robustness and consistency as a biomass proxy available for long-term, large-scale studies of phytoplankton dynamics. Alternative remote sensing products, such as particulate backscattering-derived phytoplankton carbon have limited validation, and previous tests using the carbon-based productivity model (Behrenfeld et al., 2005) in this region (Dogliotti et al., 2014) showed poor performance. Surface Chl-*a* can sometimes be decoupled from vertical biomass structure (e.g., presence of a deep Chl-*a* maximum); hence, the results of the present study will represent the dynamics of surface blooms, with some accounting of processes in the water column (using MLD and Z_{eu}, in some cases lagged to conditions previous to the bloom peak).

In this article, we investigate the effects of the light field (PAR and Z_{eu}) and MLD on phytoplankton bloom dynamics in the Southwest Atlantic, focusing on the Argentine Shelf. While the influence of light and MLD on bloom initiation has been widely studied in open-ocean environments, far less is known about how these drivers operate in spatially heterogeneous shelf systems. To address this gap, we combine reanalysis data (wind, MLD), satellite-derived products (Chl-*a*, PAR), and statistical techniques to evaluate the spatial variability of bloom phenology over two decades (1998–2019) and to assess the predictive capacity of light and MLD variables at seven representative sites across the shelf. This dual-scale approach enables us to test the extent to which classical light-stratification paradigms explain bloom timing in shelf regions and to identify where these paradigms break down. Through this work, we provide new insight into the regional controls and spatial heterogeneity of bloom phenology, which is critical for understanding ecosystem responses to environmental variability and climate change. To do so, we first characterize climatological bloom patterns and phenological metrics across the study area (Sect. 3.1), then evaluate spatial differences in the timing and structure of seasonal blooms at selected sites (Sect. 3.2), and finally assess the relationship between bloom variability and light and MLD using stepwise multiple regression analysis (Sect. 3.3).

2 Data and methods

2.1 Study area

The Southwestern Atlantic Ocean (SWAO) exhibits a rich and remarkable diversity of geo-morphological, climatic, and oceanographic features. Part of the continental shelf of this vast region can be further subdivided latitudinally into two distinct subregions (Piola et al., 2018): the Central Shelf (CS), encompassing portions of southern Brazil, Uruguay, and northern Argentina, and the southernmost Patagonian Shelf (PS), located south of $\sim 38°$ S. In this work, two of the selected sites are considered to be located in the CS because of their characteristics even though they are located $\sim 39°$ S. The CS is influenced by the continental discharge of the Río de la Plata and limited offshore by the high energy exchange area of Brazil-Malvinas Confluence, an area where the warm, salty waters of the Brazil Current meet the cold, fresh waters of the Malvinas Current. This confluence is also a region with strong currents, upwelling, and eddies (Garzoli and Garraffo, 1989; Matano et al., 2010). The atmospheric variability significantly influences the seasonal circulation patterns in the CS (Ruiz-Etcheverry et al., 2016; Strub et al., 2015). The semi-permanent South Atlantic anticyclone's southward migration during spring and summer generates southwestward alongshore winds, blocking the passage of cold fronts (Vera et al., 2002). Conversely, its northward displacement in winter increases cold front frequency, leading to northeastward winds. These atmospheric shifts substantially impact ocean circulation in this area (Forbes and Garrafo, 1988; Höflich, 1984). The PS, in turn, is constantly affected by westerly winds and a high variability in tidal range (Glorioso and Flather, 1997; Luz Clara et al., 2014; Trenberth, 1991). This part of the shelf is bounded offshore by cold, low-salinity, nutrient-rich waters of the Antarctic Circumpolar Current, which are advected northward by the Malvinas Current.

To analyze the effects of the light field (PAR and Z_{eu}) and MLD on main blooms in the SWAO, we explored the area between 34–55° S and 50–70° W (Fig. 1). In particular, seven study sites were selected to further explore the capability of environmental variables related with the light field and MLD to predict the main bloom peak. The sites were selected given their contrasting oceanographic regimes and their biological relevance (two at the south of CS and the others in the PS region) (Fig. 1, Table 1). Moreover, these sites fall within different biogeographical regions described in Delgado et al. (2023), hereafter D2023. The main relevant characteristics of each site are provided below.

- EPEA – Estación Permanente de Estudios Ambientales (EP). This is one of the Marine Ecological Time Series (METS) run by the "Dinámica del Plancton Marino y Cambio Climático (DiPlaMCC)" program from Instituto Nacional de Investigación y Desarrollo Pesquero (INIDEP). It is located in the CS, 13.5 nautical miles offshore near the 50 m depth isobath

(38.47° S/57.68° W). EPEA encounters both near-shore and continental shelf waters, with a persistent Mid-Shelf Front (MSF) often located offshore the 50 m isobath (Lucas et al., 2005; Martos and Piccolo, 1988). According to in situ sampling (period 2000–2017) the mean surface Chl-*a* for this site was 1.08 mg m^{-3} and the annual climatological maximum was observed in August (Ruiz et al., 2020).

- COSTAL-AR-4 (C4). This site corresponds to the position of station 4 of the COSTAL-AR transect, another METS maintained by DiPlaMCC sited on CS. This transect runs from the coastal sector to the continental slope in a northwest-southeast direction at ∼ 38° S. It is predominantly influenced by Subantarctic Shelf Waters, and its mid-shelf location (CS) near the 90 m isobath (38.75° S/56.25° W), between the MSF and the Shelf-Break Front, gives it a typical temperate seasonal water column stratification cycle. Existing in situ data collected at this site (1987–1989) showed a surface mean Chl-*a* of 1.71 mg m^{-3} and a maximum of 6.05 mg m^{-3} in October (Carreto et al., 1995).

- Peninsula Valdés (PV). This site is located on the PS at the PV front (42.75° S/63.00° W), one of the regions where tidal energy dissipation rates are among the highest in the Argentine Shelf (Luz Clara et al., 2015; Moreira et al., 2011; Rivas and Pisoni, 2010). This front plays a crucial role in local hydrographic dynamics, controlled by tidal currents, winds, and enhanced by inshore headlands. It typically develops during spring warming and persists until autumn when water column stratification weakens. Characterized by a strong horizontal temperature gradient, the PV front separates vertically homogeneous coastal waters from stratified offshore waters (Sabatini and Martos, 2002). This site is located on the seasonally stratified side of the front, where Chl-*a* concentration is usually high in spring-summer (Carreto et al., 1986). This region is an important fishing ground (e.g., anchovy, hake, shrimp) and a breeding and feeding place for marine mammals and birds (Giaccardi and Caloni, 2022).

- San Jorge Gulf (SJ). This site is located in the southern part of the San Jorge Gulf mouth (46.33° S/65.58° W) on the PS. The vertical structure of the water column and the circulation within the SJ gulf are conditioned by the characteristic westerly winds, and by the effect of tidal mixing (Akselman, 1996; Carreto et al., 2007; Glorioso, 1987; Guerrero and Piola, 1997). At the southern area of the gulf, a complex permanent tidal-thermohaline frontal system (in the north-south direction) is formed, representing the transition between low-salinity, tidally mixed Coastal Waters (Bogazzi et al., 2005) and the more saline, seasonally stratified waters of the continental shelf. Relatively high Chl-*a* concentrations are generally observed in spring-summer (Segura et al., 2021). The dynamics that characterize the oceanographic fronts favor primary and secondary productivity (Acha et al., 2004, and references therein). The gulf is an area rich in fishery resources, especially the Argentine red shrimp (Bertuche et al., 2000; Moriondo Danovaro et al., 2016).

- Southern Shelf Break (SS). This site is located in the southern part of the shelf break (47.77° S/60.98° W) south of the "Agujero Azul", a biodiversity rich zone that Argentina intends to declare as a marine protected area. It is part of the productive slope front, with relatively high Chl-*a* concentrations all year around, and especially high in spring-summer, where a high primary production has been estimated (Dogliotti et al., 2014; Segura et al., 2013). Therefore, this region is favorable for the Argentine squid, and a feeding ground for birds and marine mammals (Acha et al., 2024).

- Bahía Grande (BG). This site is located south of 50° S (51.00° S/67.67° W) within the Grande bay, known for its high tidal energy dissipation. The area experiences a prominent thermal front, particularly during spring and summer (Sabatini et al., 2004). This front promotes conditions conducive to large phytoplankton blooms, which support abundant zooplankton populations. As a result, BG is a significant fishing ground for Austral species, such as hoki (Cousseau and Perrota, 2004). According to Luz Clara (2008), the BG front exhibits the highest chlorophyll-*a* concentrations towards the end of the year.

- Burdwood (BW). It is located in the Burdwood Bank (54.33° S/59.75° W), a submarine plateau where powerful currents converge, creating unique physical conditions that promote water retention and plankton abundance in the area. This, in turn, facilitates the operation of the biological carbon pump along its edges. Both the biological and the microbial pumps play a crucial role in oceanic carbon sequestration, reducing atmospheric carbon dioxide (a greenhouse gas) and mitigating global warming (Martín de Nascimento et al., 2020). Picophytoplankton, especially *Synechococcus*, dominate the phytoplankton during summer (Guinder et al., 2020). Because of its high biodiversity, mainly benthic, it was declared a marine protected area called "Namuncura – Banco Burdwood".

2.2 Chlorophyll-*a* data

Satellite-derived surface Chl-*a* (mg m^{-3}) obtained from the European Space Agency's Ocean Colour Climate Change Initiative (OC-CCI) was used as a proxy of phytoplankton biomass. Level 3 Chl-*a* product at 4 km and 8 d resolution for the period 1998–2020 was downloaded

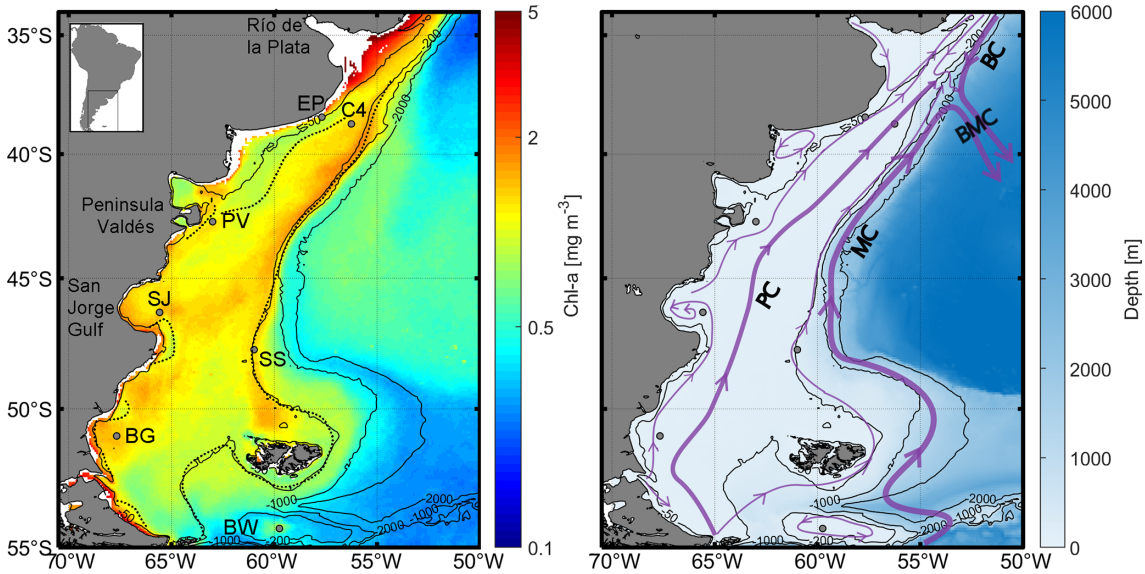

Figure 1. (left) Selected sites overlaid on the mean surface Chl-*a* concentration map from OC-CCI v6.0 (1998–2020). Schematic frontal zones in the Southwest Atlantic Ocean (SWAO) are shown as black dotted lines (based on Acha et al., 2018). Site abbreviations correspond to those listed in Table 1. (right) Bathymetry map showing a schematic surface circulation adapted from Strub et al. (2015). Black solid lines indicate the 50, 200, 1000, and 2000 m isobaths. MC: Malvinas current, BC: Brazil Current, BMC: Brazil–Malvinas Confluence, PC: Patagonian Current.

Table 1. Selected site names, location (latitude, longitude), depth (Z), and the corresponding biogeographical region (BGR) as defined in D2023.

Site		Lat (°)	Lon (°)	Z (m)	BGR
EP	Estación Permanente de Estudios Ambientales (EPEA) time-series	−38.47	−57.68	52.1	R2
C4	COSTAL-AR-4	−38.75	−56.25	90.8	R7
PV	Peninsula Valdes	−42.75	−63.00	75.9	R9
SJ	San Jorge Gulf	−46.33	−65.58	78.8	R9
SS	Southern Shelf break	−47.77	−60.98	276.8	R8
BG	Bahia Grande	−51.00	−67.67	95.6	R9
BW	Burdwood Bank	−54.33	−59.75	89.3	R1

(http://www.esa-oceancolour-cci.org/, last access: 22 July 2022) and extracted over the study area (34–55° S; 55–70° W). The OC-CCI Chl-*a* version 6 product uses remote sensing reflectance (R_{rs}) from multiple sensors (Sea-viewing Wide Field of View Sensor (SeaWiFS), MODerateresolution Imaging Spectroradiometer (MODIS-Aqua), Medium Resolution Imaging Spectrometer (MERIS), Visible Infrared Imaging Radiometer Suite (VIIRS) and Ocean and Land Colour Instrument (OLCI)) that were band-shifted and bias-corrected to match MERIS bands. Chl-*a* is calculated using the merged R_{rs} by blending multiple algorithms (OCI, OCI2, OC2 and OCx) with the weighting determined by water class memberships (14 optical classes). Although OC-CCI was originally focused on Case-1 waters, i.e., water where phytoplankton chlorophyll-*a* primarily determines the optical properties of the water, part of the in situ data used for selecting the in-water algorithms included Case-2 waters (where the optical properties vary independently of the Chl-*a*) and together with some flagging and the algorithm choice based on optical water classification, Chl-*a* retrieval in Case-2 waters are also accounted for (D4.2 – Product User Guide for v6.0 Dataset: https://climate.esa.int/en/projects/ocean-colour/key-documents/, last access: 12 January 2023; Sathyendranath et al., 2019). Even though some sparse in situ Chl-*a* data exists in this region (e.g., EPEA time series), it only provides qualitative support for the temporal behavior of the satellite-derived chlorophyll, despite scale differences, which make it difficult to quantitatively assess accuracy in the representation of the seasonal signal. The OC-CCI 8 d product is derived from globally merged and bias-corrected reflectance data that are processed consistently over space and time using the same algorithms and quality-control procedures. Its performance has been evaluated against a large, globally distributed in situ dataset ($N = 15\,599$; Valente et

al., 2019), showing good overall agreement when all matchups are pulled together ($R^2 = 0.78$, RMSE $= 0.98\,\mathrm{mg\,m^{-3}}$; $N = 15\,599$, Yu et al., 2023). This RMSE represents a global aggregate statistic spanning a wide range of chlorophyll concentrations and water types and should not be interpreted as a uniform or local uncertainty. In relative terms, chlorophyll retrieval uncertainties are consistent with commonly reported values (i.e., about 30 %) for satellite-derived products. This uniform processing ensures that relative variations, such as those describing the seasonal and interannual behavior of Chl-*a*, are expected to be reliable across regions. The 8 d, rather than daily, temporal resolution product was selected to reduce data gaps while retaining the ability to detect the main phytoplankton bloom with adequate accuracy and precision (Ferreira et al., 2014; Racault et al., 2014). To further reduce remaining gaps, which are most prominent during winter at higher latitudes, a three-step gap-filling procedure was applied (Racault et al., 2014), using spatial interpolation within a 3×3 pixel window followed by temporal interpolation from adjacent weeks when available.Under persistently low-light or cloudy conditions, phytoplankton can photoacclimate by increasing intracellular chlorophyll content, which alters the relationship between chlorophyll concentration and biomass and may bias surface chlorophyll as a biomass proxy (e.g., Begouen Demeaux et al., 2025). Such physiological adjustments can influence the magnitude of chlorophyll variability, particularly at short timescales. However, the phenological metrics considered here, i.e., bloom initiation, peak timing, and termination, are based on sustained changes in chlorophyll concentration over multi-week to seasonal timescales, which primarily reflect biomass accumulation and loss. In addition, in the southern part of the study area, gap filling is most prevalent during winter, whereas the main surface blooms occur in spring and summer, when light conditions improve and data coverage is higher. Consequently, the influence of photoacclimation-related biases on the detection and timing of the principal bloom events analyzed here is expected to be limited.To ensure consistency with the environmental datasets, the chlorophyll data were resampled to 9 km resolution, and shallow coastal waters (depth < 20 m), where standard chlorophyll algorithms are known to perform poorly, were masked..

2.3 Environmental variables

The following environmental variables related to the light and the stability of the water column were used to evaluate the major mechanisms driving phytoplankton dynamics. The Photosynthetically Available Radiation (PAR) incident at the surface is the mean daily irradiance, i.e., photon flux density, in the visible range (400 to 700 nm) that can be used for photosynthesis. The 8 d and 4 km spatial resolution merged PAR product provided by GlobColour project and distributed by ACRI-ST (https://hermes.acri.fr/, last access: 30 July 2022) was downloaded. This PAR product (mol quanta $\mathrm{m^{-2}\,d^{-1}}$) results from merging the original Level 2 products from MODIS, SeaWIFS, and VIIRS (NPP and JPSS-1) sensors (Frouin et al., 2003). The euphotic depth (Z_{eu}) was defined here as the depth receiving 1 % of surface photosynthetically available radiation (PAR). Although this threshold does not represent a strict physiological cutoff, and photosynthesis and phytoplankton biomass may occur below this depth, it provides a widely used operational measure of the vertical extent of the light environment most relevant to surface bloom development. In the Argentine Sea, field observations indicate that during periods of surface bloom growth and peak biomass, light is strongly attenuated within the upper layer due to high phytoplankton concentrations, limiting net community growth at greater depths (Lutz et al., 2010; Segura et al., 2013; Dogliotti et al., 2014). Consequently, Z_{eu} offers a practical descriptor of vertical light limitation when assessing the interaction between light availability and mixed layer depth in controlling bloom phenology. While Z_{eu} provides a consistent and widely used descriptor of vertical light limitation, the absolute irradiance at this depth can vary substantially across sites and seasons, particularly at higher latitudes. Because phytoplankton respond to absolute light levels rather than to a fixed fraction of surface irradiance, the same relative threshold (e.g., 1 % of surface PAR) may correspond to very different physiological conditions in winter versus summer. In this study, however, the focus is on the enhanced surface biomass accumulation associated with bloom development, rather than on depth-resolved physiological responses. Accordingly, Z_{eu} is used here as an operational metric that enables consistent spatial and temporal comparisons of light limitation across the region. For this purpose, Z_{eu} was calculated from satellite data assuming a constant attenuation coefficient and optically homogeneous waters. Two parameterizations (Morel et al., 2007), using either satellite-derived Chl-*a* or the attenuation coefficient at 490 nm ($K_d(490)$) were first evaluated using Z_{eu} calculated from in situ PAR profiles (Biospherical PUV-500/510B) collected at EPEA time series (DiPlaMCC – INIDEP) in the period 2000–2016 ($n = 41$). The merged Level 3 $K_d(490)$ product at 4 km and 8 d resolution for the period 1998–2020 was obtained from the European Space Agency's OC-CCI. The parameterization using $K_d(490)$ as input, with the layer thickness set to $1/K_d(490)$, yielded better results. Although both models had a slope close to 1 (type-2 linear regression), the Chl-*a*-based model showed a lower coefficient of determination, larger positive bias (overestimation), and higher scatter ($R^2 = 0.71$, bias $= 23.6$ %, APD $= 25$ %) compared to the $K_d(490)$-based model ($R^2 = 0.79$, bias $= -1.1$ %, APD $= 10.7$ %). Consequently, Z_{eu} modeled using the OC-CCI $K_d(490)$ product was adopted for the present study. Mixed layer depth (MLD) data were obtained from the Copernicus Marine Environment Monitoring Service (CMEMS) GLORYS12V1 reanalysis product (Lellouche et al., 2021). GLORYS12V1 is a global ocean eddy-resolving model with a uniform horizontal

grid spacing of 1/12° and 50 vertical levels. The MLD within this dataset is determined by identifying the depth at which the temperature gradient exceeds a threshold of 0.1 °C m^{-1}. The 10 m zonal (U) and meridional (V) wind component gridded fields were obtained from the Copernicus Climate Data Store (https://marine.copernicus.eu/, last access: 15 August 2022) for the ERA5 reanalysis product. The wind-curl and wind intensity fields were computed from U and V. The wind data is provided at hourly temporal resolution and a 0.25° spatial resolution. ERA5 is the fifth-generation atmospheric reanalysis produced by the European Centre for Medium-Range Weather Forecasts (ECMWF). It integrates atmospheric observations from various sources with a global circulation model to create a temporally consistent and spatially complete dataset. To ensure consistency and comparability, all environmental variables were re-gridded to match the spatiotemporal resolution of Chl-*a* data (9 km, 8 d).

2.4 Ecological and physical indices

To study the phytoplankton dynamics and the major environmental drivers affecting them, different ecological and physical metrics were estimated (Table 2) based on the phenological parameters defined by Platt and Sathyendranath (2008). In the present study we focus on the main bloom event of the year, defined as the Chl-*a* maximum within a 12-month period (year) and the bloom initiation was determined using the threshold method. The yearly or climatological median of the Chl-*a* time series was calculated and the bloom start date was identified as the first point at which the Chl-*a* level raised a certain percent above the median. The biomass-based threshold method defines bloom onset based on anomalies relative to a climatological baseline, rather than on absolute values, minimizing possible systematic biases and residual inter-sensor differences in the blended Chl-*a* OC-CCI product and enhancing the robustness of bloom onset detection. This approach helps ensure that bloom detection is driven by meaningful ecological departures rather than noise or retrieval error. A threshold of 5 % above the median value was used to be consistent with previous phytoplankton phenology studies (e.g., Ferreira et al., 2021; Krug et al., 2018; Racault et al., 2012; Siegel et al., 2002). And as in Siegel et al. (2002), we found little quantitative differences and consistent spatial and interannual patterns in the analyzed phenological metrics, when different thresholds (i.e. 3 % and 7 %) were tested (not shown). Given that we focus on the main bloom, the time of the yearly or climatological Chl-*a* maximum is first found (TB_{peak}), then going backwards from that point the first value above the 5 % threshold was identified as the bloom initiation time (TB_{init}), and going forward the first value closer to the Chl-*a* maximum (B_{peak}) before the Chl-*a* levels go below the threshold was identified as the time of the bloom termination (TB_{end}). Mean phenological metrics between 1998 and 2019 were first calculated for the whole region by calculating for each pixel the average of the Chl-*a* concentration for each 8 d image during the 1998–2019 period thus obtaining a mean annual cycle ($n = 46$) for each pixel. In turn, the same metrics were calculated using the full Chl-*a* time series ($n = 46 \times 22 = 1012$) at the 7 selected sites, thus a time series of the estimated metrics for each year ($n = 22$). Using the same fixed 12-month period (year) to examine the phytoplankton growth cycle for all the areas where the primary bloom occur at different seasons can be unsuitable (Racault et al., 2012). In the southern regions (>39° S) blooms usually occur late (December) or early (January–February) in the year, therefore using the fixed conventional calendar year can lead to inconsistent estimation of the main bloom. Consequently, for the sites located north of 39° S (EP and C4), the conventional calendar year (January–December) was used, while a 1-year temporal window from June to May was applied for sites south of 39° S, i.e., PV, SJ, SS, BG and BW. In turn, given that most of the study area is located in the southern region, the Jun-May definition was used to calculate the climatological metrics over the whole region.

Physical indices were derived from PAR, MLD and Z_{eu} datasets. The ratio between Z_{eu} and MLD (Z_{eu} : MLD) was estimated. This ratio is an index that helps quantifying the concept that phytoplankton growth would be favored when light penetrates deeper than the mixed layer, i.e., Z_{eu} : MLD > 1 (Sverdrup, 1953). Cushing (1989) referred to it as the "production ratio" and linked it to the ability of different phytoplankton groups to dominate under varying ratio values.

2.5 Statistical analysis

Stepwise linear regression (SWLR) analysis was used to explore the capability of different variables to predict the main bloom peak at seven selected sites in the Argentine continental shelf. SWLR is a predictor selection method that iteratively applies forward and backward linear regression to determine a final linear model. At each step, a predictor is either included or removed based on statistical significance, so that only meaningful predictors are retained in the final model. The selection process is guided by partial F tests, which evaluate whether the inclusion of a predictor significantly improves the model fit (Yang et al., 2017). Specifically, the F-statistics compares the variance explained by the model with and without the predictor, using thresholds for F-to-enter and F-to-remove of 0.05 and 0.10, respectively. If the computed F-value exceeds the critical threshold, the predictor is included in the model. SWLR is considered a useful analytic tool when predictors may not be statistically independent since it avoids collinearity among the predictors and develops a reliable regression model (González-Reyes et al., 2024). Machine learning methods were not considered for this analysis because they require large datasets for training and testing the models while the available data used in this study was scarce at the interannual scale. A brief description of the SWLR steps is provided in Torres et al. (2024).

Table 2. Ecological and physical metrics.

Metric	Description	Unit
TB_{init}	Time (8 d) of the main bloom initiation	week
TB_{peak}	Time (8 d) of the main bloom peak	week
TB_{end}	Time (8 d) of the main bloom end	week
B_{peak}	Maximum Chl-*a* (main bloom peak)	$mg\,m^{-3}$
PAR	Photosynthetically Available Radiation	$mol\,quanta\,m^{-2}\,d^{-1}$
MLD	Mixed Layer Depth	m
Z_{eu}	Depth of the euphotic zone	m
Z_{eu} : MLD	Z_{eu} to MLD ratio	–
U-wind	Zonal wind speed	$m\,s^{-1}$
V-wind	Meridional wind speed	$m\,s^{-1}$
Wind-curl	Wind curl	s^{-1}

The SWLR analysis has been used in quantification of linear linkages between factors and response (Li et al., 2021), and forecasting science (Ribeiro Torres et al., 2024; and references therein). The analysis included the average values of MLD and wind speed over the 2- and 4-week periods preceding the bloom peak. These temporal aggregates were computed to capture phytoplankton growth responses to MLD shoaling and wind-driven nutrient input, without being too close or too far from the peak so as to dilute the influence of immediate pre-bloom forcings. To avoid spurious results caused by the seasonal variability observed in the time series of physical variables and Chl-*a*, we removed the seasonal cycle by subtracting the weekly climatology from the data. In addition, due to the large dissimilarities in the variability range, we standardized the time series previous to the stepwise linear regression (SWLR) analysis. Hence, all the predictors and B_{peak} time series have zero mean and unit variance. Moreover, the normalization of time series allows for the qualitative identification of the explained variance importance of each predictor (Aiken, 1991) through the analysis of the model's coefficients (a larger coefficient indicates a higher explained variance).

The predictors (inputs) considered in the analysis included 8 d mean U-wind, V-wind, wind speed, and wind-curl; 8 d mean MLD, PAR, Z_{eu}, and Z_{eu} : MLD ratio, all measured at the time of the main bloom peak (TB_{peak}). To capture pre-bloom conditions, we also included the mean values of these predictors over the two and four weeks leading to TB_{peak}, denoted by subscripts $_2$ and $_4$, respectively. For example MLD_2 represents the average MLD over the two weeks prior to the bloom peak. The response variable is the standardized non-seasonal Chl-*a* anomaly at the peak, denoted B'_{peak} in the following.

The SWLR model was expressed as follows:

$$\tilde{B}'_{peak} = \sum_{i=1}^{m} \beta_i X_i + \epsilon, \quad (1)$$

where β_i are the regression coefficients, X_i are the selected predictors, ϵ is the residual error, and m is the number of selected predictors. Note that the statistical model has no intercept because all the variables, including, the response variable, are standardized. The model's performance in predicting B_{peak} anomalies was evaluated using two metrics: the explained variance (R^2) and the root mean square error (RMSE). The R^2 statistic quantifies the proportion of variance in B'_{peak} explained by the model, while RMSE measures the average prediction error.

3 Results

3.1 Bloom climatology

Figure 2 illustrates the 22-year climatological annual cycle of key phenological phases of the phytoplankton bloom cycle across the study area: time of the bloom initiation (TB_{init}) and bloom peak (TB_{peak}), and mean maximum chlorophyll-*a* concentration (B_{peak}). The spatial distribution of these phases provides insights into the variations in bloom dynamics across the region, highlighting the influence of oceanographic and climatological conditions.

TB_{init} varies significantly across the study area, with earlier initiation in the Central Shelf (CS) and later initiation in the Patagonia Shelf (PS). In the CS region, TB_{init} typically occurs in May north of 35° S, and between July and September between 35 and 39° S, likely due to higher light levels and shallow mixed layers that enable sufficient light penetration for early phytoplankton growth. As winter transitions into spring, increased solar radiation and reduced vertical mixing create favorable conditions for bloom onset. A slightly different situation occurs near the coast (depth < 50 m), where bloom initiates even earlier in autumn (around April). On the other hand, the PS region, influenced by colder, nutrient-rich waters mostly of Subantarctic origin, experiences a delayed TB_{init}, generally from September to November, attributed to the thermal inertia of the water column. In these Subantarctic waters, deeper winter MLD retain a greater heat capacity, requiring a longer accumulation of net solar radiation in spring

to achieve thermal stability. Consequently, these cold, voluminous layers require more time to warm and this delays the onset of water column stratification, which in turn prolongs the period where phytoplankton cells are mixed below the euphotic zone. This mechanism results in a later TB_{init} compared to the northern and mid-shelf regions, where warmer waters and shallower winter MLD permit stratification to develop earlier in the spring.

The timing of the bloom peak (TB_{peak}) follows the pattern of TB_{init}, with peak timing occurring earlier in the CS than in the PS. In the CS region, TB_{peak} is typically reached by September to November, reflecting the rapid response of phytoplankton to favorable light and nutrient conditions following TB_{init}. Shallow mixed layers in this area further enhance light penetration, promoting an early peak. Near the coast, the peak occurs in autumn and winter months, probably related to phytoplankton communities adapted to low light and turbulence, as will be explained later (Sect. 3.2).

In the PS region, however, TB_{peak} is mostly delayed to December or January, in line with the latter TB_{init}. The dependency on seasonal warming and water column stratification, as well as the influence of Subantarctic waters and the Malvinas Current, prolongs the conditions needed for peak phytoplankton growth in this colder region. This later peak timing is consistent with the PS's need for extended periods of sunlight to support high phytoplankton productivity.

The bloom intensity (B_{peak}) also varies greatly across the study area (Fig. 2). The highest B_{peak} values are observed along the southern PS and near frontal systems (see locations in Fig. 1 left), where nutrient-rich upwelling and favorable light conditions sustain high chlorophyll-*a* concentrations. In contrast, offshore regions farther from nutrient sources exhibit lower B_{peak} values. In these deeper waters, nutrients are scarce, and strong winds drive deeper mixed layers, causing phytoplankton cells to be continuously mixed below the euphotic zone. As a result, they do not remain in the sunlit layer long enough for optimal growth.

3.2 Bloom phenology at selected sites

The timing of the main phytoplankton bloom peak (TB_{peak}) differed between northern and southern sites, as mentioned in the previous climatological section. At the two sites located in the north of the study region, EP and C4, the B_{peak} occurred most frequently in autumn and winter (Fig. 3). On the other hand, at southern sites the main bloom predominantly occurred in spring and summer.

At EP, a coastal site, the climatological Chl-*a* phenology showed a distinct pattern, with the main bloom extending from end of March to end of June and peaking by the end of May (Fig. 4), being on average the lowest B_{peak} ($1.36\,mg\,m^{-3}$) compared to the other sites analyzed. It is worth noting that the timing of the main bloom showed high variability, being the highest and equally frequent in both May and October while also occurring in other months, except in July (Fig. 3). The mean main bloom at this site occurred in autumn and Chl-*a* values stayed relatively stable around $\sim 1\,mg\,m^{-3}$ in winter (Jul-Sep) coinciding with a deeper MLD (i.e., the water column was practically mixed up to the bottom) and the lowest incident PAR and Z_{eu}, being thus the Z_{eu} : MLD ratio also low ($\ll 1$). At the beginning of spring (end of Sep), a secondary peak can be observed as the PAR increases and the MLD shallows. Then the phytoplankton biomass (parameterized by Chl-*a*) starts decreasing in spring and reaching the lowest values in summer ($<1\,mg\,m^{-3}$) when the MLD is shallow, PAR and Z_{eu} are high and the Z_{eu} : MLD is $\gg 1$. Field studies at this site have reported that during the cold period there is a dominance of micro-phytoplankton, especially large diatoms that are able to grow in low light turbulent environments; while during summer the community is dominated by ultra-phytoplankton, especially cyanobacteria that are adapted to take advantage of the low nutrient regime imposed by a stratified water column (Ruiz et al., 2020; Silva et al., 2009). Compared to the other sites, EP showed the highest inter-annual variability in the time of initiation, peak and end of the main bloom (Fig. 5). From the 22 years considered, only in 7 cases the TB_{peak} occurred within the climatological timeframe. In 14 cases the duration was shorter than, or hardly reached, 2 months. Regarding B_{peak}, it ranged between 1.2 and $3.3\,mg\,m^{-3}$, and in 9 years B_{peak} was higher than $2\,mg\,m^{-3}$.

At C4, the main bloom occurred most frequently in September (50 %), but it also occurred in other months, with October and December being the second and third most frequent months (Fig. 3). The C4 site, located on the shelf, showed characteristics of a temperate regime. Climatologically, the bloom extends from mid-July to the beginning of December, peaking in September and remaining with high Chl-*a* until November (Fig. 4). At the mean TB_{peak} (end of winter–beginning of spring), the MLD was slowly becoming shallower (water column stratification was beginning to develop) and PAR and Z_{eu} were slowly increasing; as a consequence, the Z_{eu} : MLD ratio also slowly increased (climatologically getting closer to ~ 1); all of which provided good conditions for the growth of phytoplankton, consistent with Sverdrup's theory (Sverdrup, 1953). In turn, during summer (January–March), phytoplankton biomass was limited presumably due to the low nutrient availability and grazing pressure. At this site the inter-annual variability was not too high, showing high consistency in the timing at different years compared to the climatological period, i.e., the TB_{peak} occurred within the climatological period in 19 of the 22 years. In 2012 two Chl-*a* peaks occurred with very similar intensity, one in May ($3.38\,mg\,m^{-3}$) and one in mid-September ($3.36\,mg\,m^{-3}$), the latter occurring within the climatological period (Fig. 5). In turn, the B_{peak} range was wide, varying between 1.6 and $10.1\,mg\,m^{-3}$, and higher than $4\,mg\,m^{-3}$ in 13 out of the 22 years.

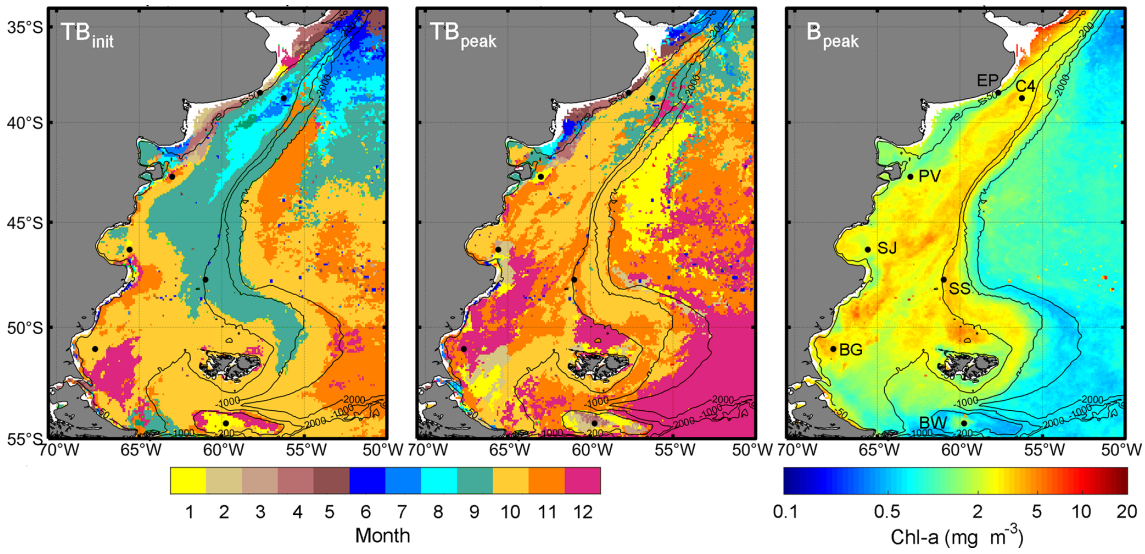

Figure 2. Mean time of the year (month) of the main bloom initiation (TB_{init}), peak (TB_{peak}) and mean maximum Chl-*a* (B_{peak}). Black lines indicate 50, 200, and 2000 m isobath contours.

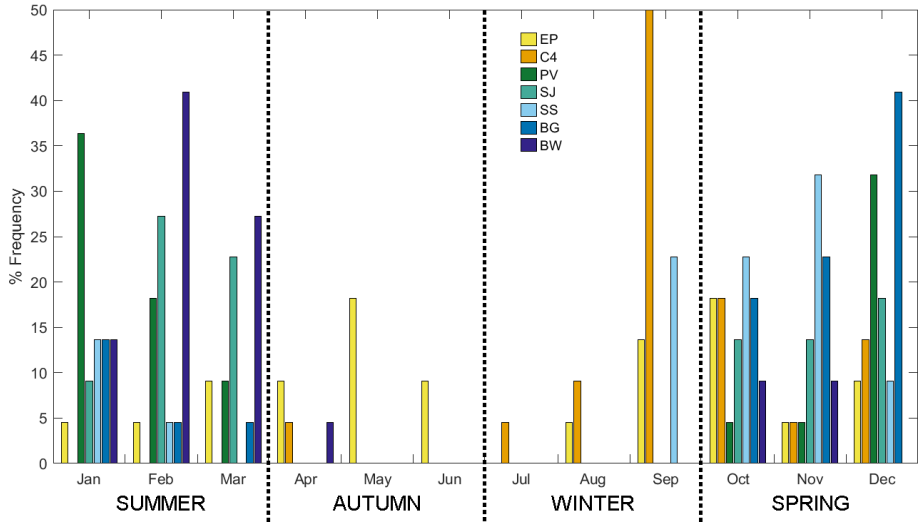

Figure 3. Frequency of occurrence, for the studied period (1998–2019), of the main bloom peak at each site per month.

At PV, the main bloom occurred in spring and summer (Fig. 3), most frequently in January (37 %) and closely followed by December (32 %). The mean climatological bloom extended from November to the end of April (Fig. 4) and peaked in January, when the water column was strongly stratified (shallow MLD). This stratification keeps phytoplankton on the illuminated upper layer (high PAR, deep Z_{eu}, and high Z_{eu} : MLD ratio), and it is probably maintained by the input of nutrients across the oceanographic front (Carreto et al., 1986; Lutz and Carreto, 1991). There is a high consistency in the timing of TB_{peak} in all the years (Fig. 5) compared to the range of climatological duration (beginning of November–end of April). The duration of the bloom was at least 4 months in 8 of the 22 years, with only 3 years in which it lasted slightly more than 1 month. The B_{peak} range was wide, varying between 1.6 and 9 mg m^{-3}, but B_{peak} was lower than 3.8 mg m^{-3} in 14 years.

At SJ, B_{peak} occurred most frequently in February (42 %), followed by March (27 %) (Fig. 3). At this site, located on a front at the south bank of the San Jorge Gulf (Fig. 1), the bloom extended from October to April (Fig. 4), peaked in February, and high concentrations of Chl-*a* are maintained approximately from end-November until end-March, probably due to the favorable conditions provided by the front, i.e., vertical stability, allowing the cells to stay in the euphotic zone (shallow MLD, high PAR, high ratio Z_{eu} : MLD), and

horizontal input of nutrients (Akselman, 1996; Segura et al., 2021). At SJ there was also a high consistency in the timing of the main bloom in all the years and the mean climatology, i.e., the B_{peak} occurred within the climatological duration of the bloom (late October–early April). The range of B_{peak} values was between 2.2 and 7 mg m^{-3}, and B_{peak} was below 4 mg m^{-3} in half of the years.

At SS, B_{peak} occurred most frequently in November (32 %), followed by September and October (24 %) (Fig. 3). At this site, located at a southern zone of the shelf-break front, the climatological bloom extended from September to March and peaked at the beginning of November (Fig. 4). At the time of the peak, the incident PAR was high, MLD was shallow, and the Z_{eu} : MLD ratio was around 1. Again, at this site phytoplankton biomass was relatively high in spring and summer (until the end of February), probably given the input of nutrients from the Malvinas Current across the front (Carreto et al., 2007). Also, at this site there was a high consistency and in all of the years TB_{peak} occurred within the climatological duration of the bloom (September–March). The B_{peak} range was between 2.7 and 9.8 mg m^{-3}, and B_{peak} was higher than 5.2 mg m^{-3} in approximately half of the years.

At BG, B_{peak} occurred more frequently in December (41 %), followed by lower frequencies in November (23 %) and October (19 %) (Fig. 3). At this site, the bloom had a relatively short temporal duration, initiating in mid-October and ending by the end of January with a constrained, but high ($\sim$ 3.8 mg m^{-3}) climatological Chl-*a* peak around the beginning of December (Fig. 4). Here, the effect of a circulation front (Carreto et al., 2018; Sabatini et al., 2004; Segura et al., 2013) was probably a source of nutrients. At the time of the bloom peak, PAR was the highest, MLD the lowest, and the Z_{eu} : MLD ratio was slightly >1. The B_{peak} occurred most of the years within the climatological duration, except in 2016 and 2019 when B_{peak} occurred later, i.e., in February and March, respectively. The range of B_{peak} varied between 2.1 and 20.4 mg m^{-3}, and B_{peak} was higher than 6.5 mg m^{-3} in 8 out of the 22 years.

At BW, the maximum Chl-*a* concentration occurred more frequently in February (41 %) and March (26 %) (Fig. 3). At this site, the bloom extended from the end of December until the end of April, reaching a climatological peak at the beginning of April, but with a plateau of relatively high Chl-*a* values from the end of January until beginning of April (Fig. 4). Consequently, the phytoplankton biomass increased in autumn, when PAR was decreasing, vertical mixing was increasing (MLD was getting deeper), and the Z_{eu} : MLD ratio was <1. There was also a good consistency between the bloom timing in the different years and the climatological cycle. B_{peak} ranged between 1.1 and 3.9 mg m^{-3} and Chl-*a* was higher than 2.1 mg m^{-3} in 15 out of the 22 years. It is worth mentioning that in winter (between May and end of July) there is no satellite-derived Chl-*a* data at this latitude (grey area in Fig. 5) given that regions with high sun zenith angles ($>70°$) are masked in the standard processing.

In a recent work, D2023 proposed the partition of the SWAO into nine biogeographical regions based on the temporal variability of Chl-*a* concentration and Self-Organizing Maps (SOM) analysis using a similar satellite-derived Chl-*a* data set (GlobColour Project). The timing, values and ranges found in this work for the selected sites are similar to the mean values for the corresponding regions reported in D2023, while some discrepancies were found at EP. It is worth noting that this site showed a high interannual variability in timing and B_{peak} values and that the region in D2023 where EP is located (R^2) includes different and disconnected areas, i.e., the northern inner shelf waters and the oceanic waters outside the shelf-break (north of 44° S), which can explain the differences found.

3.3 Modeling the main bloom

The explained variance (R^2) of the SWLR models for the standardized Chl-*a* anomaly at the peak, B'_{peak}, differed at the different sites. In almost all of the sites the SWLR model explained more than 70 % (reaching 92 % in SJ) of the variance in B'_{peak}, except in the BG site ($R^2 \sim 0.46$). Different variables resulted in good predictors of B'_{peak} depending on the site (Table 2). The main predictors are analyzed and discussed separately for each site.

At EP, the SWLR model explained $\sim$ 72 % of the variance of B'_{peak} (Fig. 6), Z_{eu} is the best predictor, followed by U-wind, both showing an inverse relationship (negative coefficients) with B_{peak} anomaly (Table 2). The Z_{eu} contribution at the time of the peak can be related to the fact that the highest Chl-*a* levels are typically reached in late winter or early spring when the water column is mixed (deep MLD). This intense vertical mixing suspends more material (Lutz et al., 2006; Ruiz et al., 2020), reducing light penetration (lower incident PAR) and, consequently, shallowing the Z_{eu}. On the other hand, the inverse relation with U-wind indicates that weaker westerly winds are associated with favorable conditions for phytoplankton growth. The RMSE ($\sim$ 0.55) highlights the relative deficiency of the linear model in representing the peak intensity in some cases (Fig. 6).

At C4, the SWLR showed an R^2 value close to 0.75, suggesting a good skill of the linear model in representing the interannual variability of the B'_{peak}. However, the RMSE value ($\sim$ 0.52) evidenced that the linear model was not able to efficiently capture the peak intensity in several cases. The main predictors that modulate B'_{peak} variability are the Z_{eu} : MLD ratio, followed by its mean value in the preceding 4 weeks (Z_{eu} : MLD_4), both of which denote an inverse relationship with the response variable. This is consistent with the climatological analysis according to Sverdrup's theory (i.e., phytoplankton growth depends on the balance between Z_{eu} and MLD).

At PV, the SWLR model explained $\sim$ 73 % of the variance in B'_{peak} (Fig. 6), Z_{eu} (negative) being the only relevant predictor able to explain the anomalies. At this site, located on

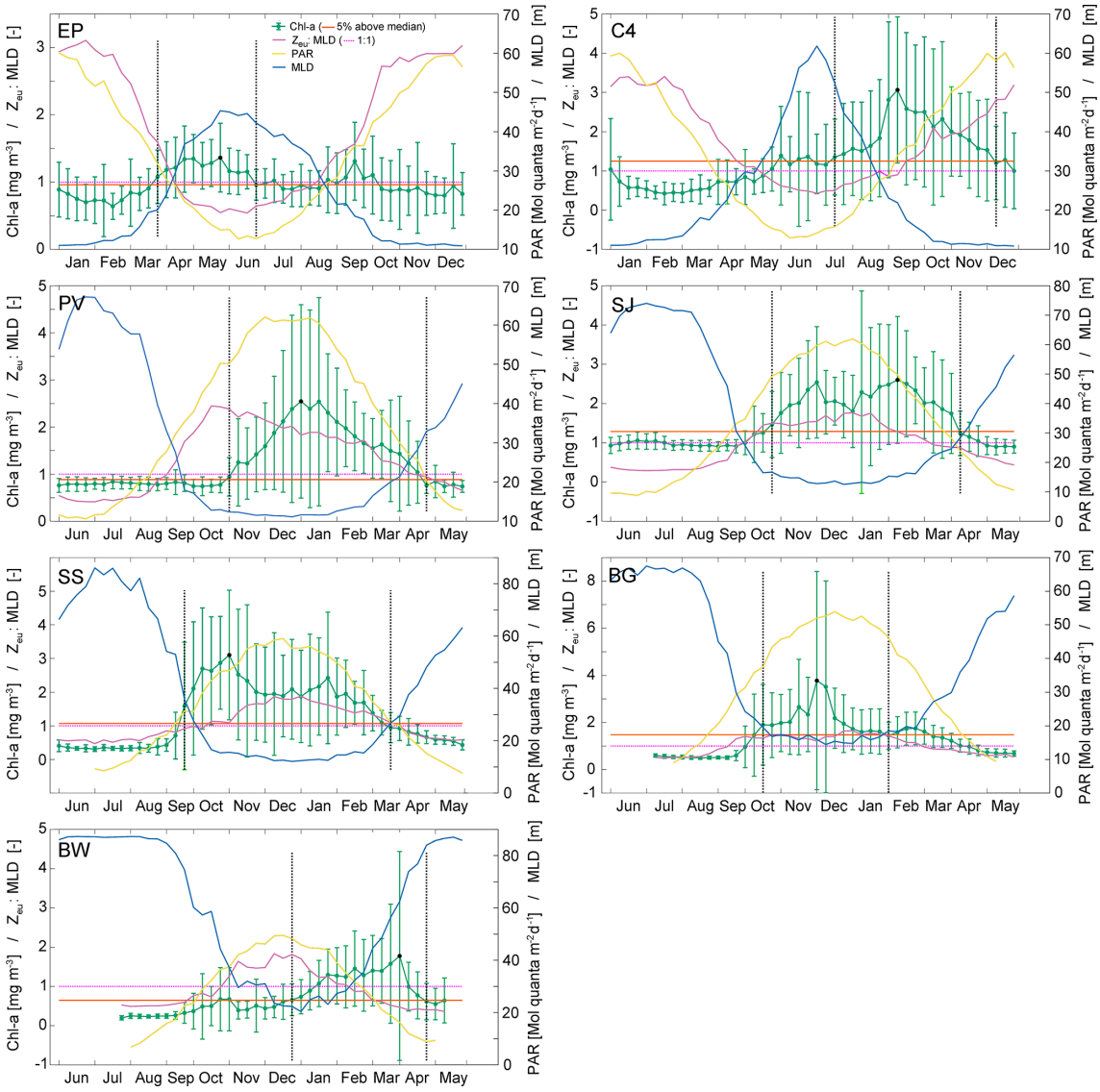

Figure 4. Annual climatology of surface Chl-a [mg m^{-3}] (bars show standard deviation), Z_{eu} : MLD, surface PAR [mol quanta m^{-2} d^{-1}], and MLD [m] at each site. Average maximum Chl-a, start and end of main bloom are indicated with a black dot and vertical dashed lines, respectively. Notice that the cycle at EP and C4 are plotted from January to December while for the other sites it is from June to May.

the stratified side of a tidal front, environmental characteristics were probably quite similar throughout the years, and the inverse relationship between the depth of the euphotic layer and the intensity of the bloom peak may be due to the attenuation of light by the phytoplankton itself producing the shallowing of Z_{eu}. The RMSE ~ 0.53 reflects the mismatch in some cases.

At SJ, the SWLR had the highest R^2 compared to the other sites (~ 0.92) in the prediction of B'_{peak} (Fig. 6). Here several predictors were relevant to explain the B_{peak} anomalies. The largest contribution to B'_{peak} was given by Z_{eu}, followed by Z_{eu} : MLD$_4$, PAR and U-wind$_2$; three of them were related to light (negative Z_{eu} and Z_{eu} : MLD$_4$ and positive PAR), and one to wind (negative U-wind$_2$). This would indicate that when the intensity of the bloom is higher, Z_{eu} is shallower due to self-shading by phytoplankton; in the same sense in the month previous to the bloom peak the ratio Z_{eu} : MLD$_4$ was low, i.e., as MLD becomes shallower (favoring water column stratification) the growth of phytoplankton would shallow the Z_{eu}. The positive relationship with PAR, which would be expected always, becomes significant at this site. The negative relationship with U-wind$_2$ suggests weakened westerly winds within the two weeks preceding the bloom peak, would favor water column stratification. Here the match between observed and modeled B'_{peak} was good in most of the cases (RMSE = 0.31).

At SS, the SWLR had a high $R^2 \sim 0.87$ (Fig. 6) with the following relevant predictors explaining B'_{peak} in order of im-

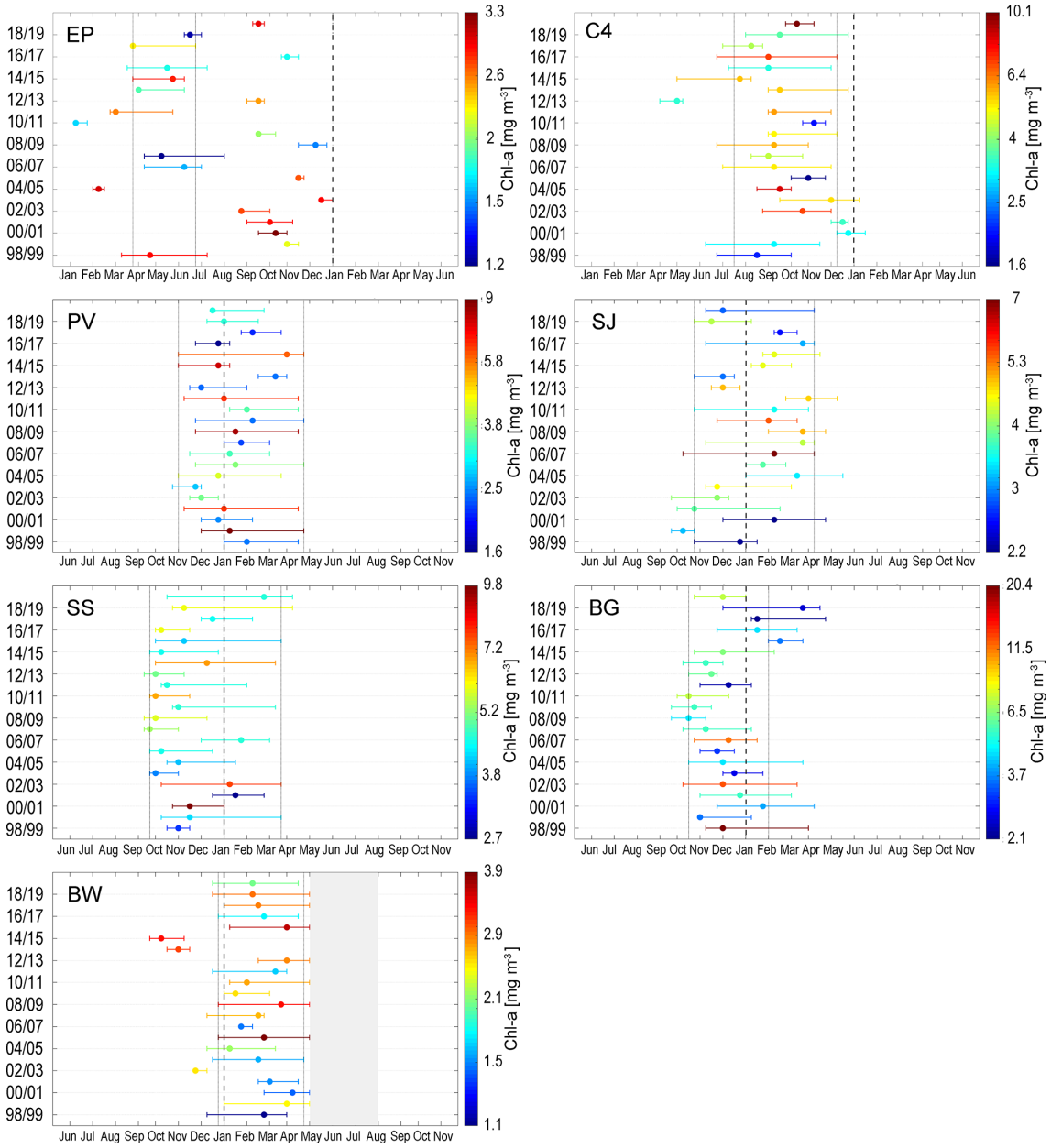

Figure 5. Interannual variability of timing (initiation, peak and ending) of the main bloom at each site. The average time of start and end of the main bloom are indicated with vertical dotted lines and the beginning of the year with a vertical dashed line. Notice that the cycle at EP and C4 are plotted from January to December while for the other sites it is from June to May.

portance: Z_{eu} : MLD, MLD, and Z_{eu} : MLD_2, all of which had negative contributions. Hence at this site, located on the outer shelf immediately connected to the shelf-break front, the variations in bloom intensity were related with the interplay between light and vertical mixing, as well as to their evolution previous to the peak. The B'_{peak} was higher when the ratio of Z_{eu} : MLD was lower, i.e., the growth of phytoplankton would shallow the Z_{eu} at the time of the peak. The same effect, though with a lower contribution, was observed regarding the values of this ratio in the two weeks previous to the peak (Z_{eu} : MLD_2) and when MLD was relatively shallower, favoring the maintenance of the phytoplankton in the lit layer. Here the match between observed and modeled anomalies in B'_{peak} was generally good in all the years (RMSE = 0.39).

At BG, the SWLR had the lowest predicting capability ($R^2 \sim 0.46$) of B'_{peak} (Fig. 6). Here only two predictors, negative Z_{eu} : MLD_2 and positive Z_{eu4}, were relevant to explain B'_{peak}; Z_{eu} : MLD_2 being the main contributor. At this site, located at the stratified side of a circulation front in Grande

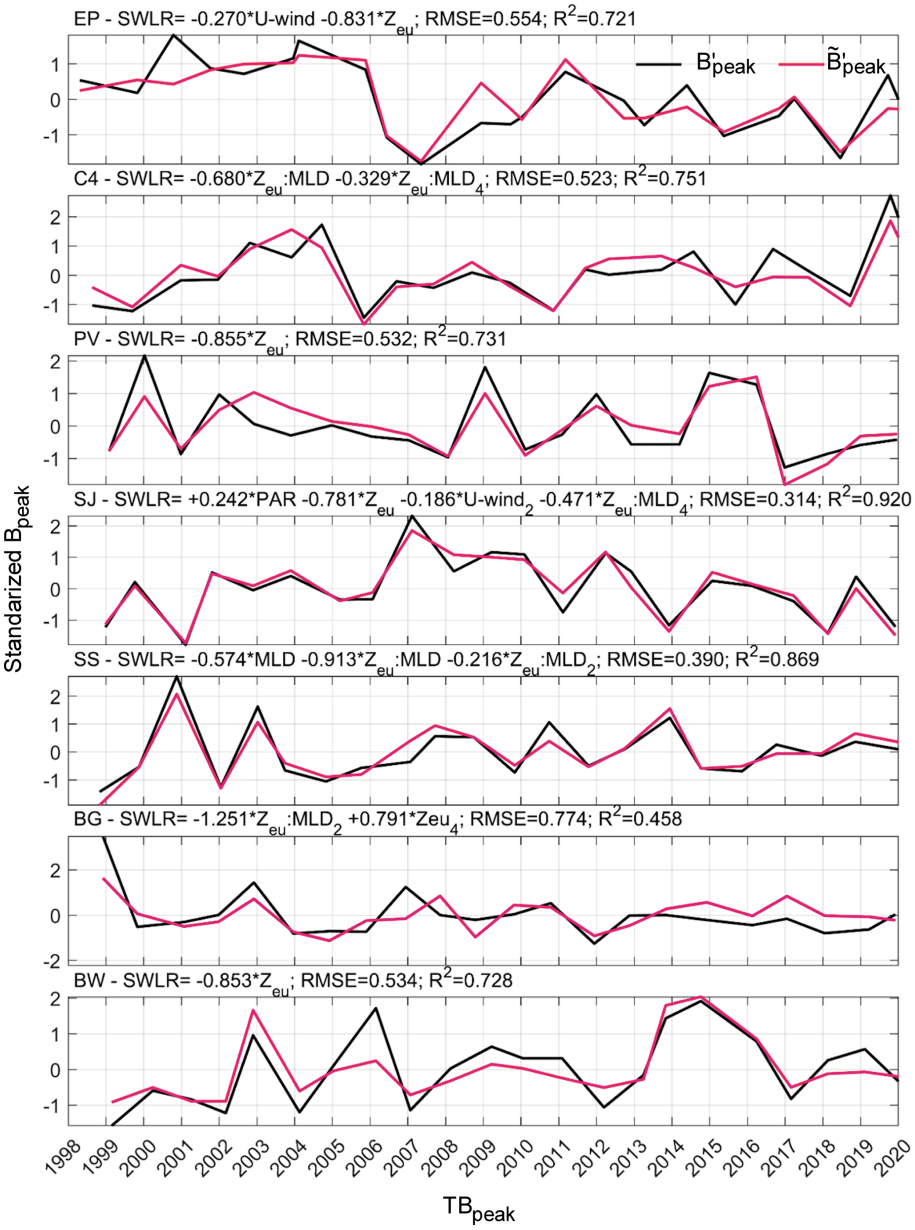

Figure 6. Satellite (black line) and modeled (red line) B_{peak} anomalies, B'_{peak}, at each site. Model equation, root mean square error (RMSE) and coefficient of determination (R^2) are shown in the figure.

Bay, the light history related to the depth of the euphotic zone previous to the bloom contributed to explain variations in B'_{peak}; when the values of $Z_{\text{eu}} : \text{MLD}_2$ were lower (competition between the shallowing of the mixed layer and euphotic depth also probably getting shallower due to phytoplankton growth) in the two preceding weeks to the peak, its intensity was higher; while the positive relationship with Z_{eu4} would indicate that light penetration had to increase in the month previous to the peak for it to have higher values. Note that this model was capable of explaining only 46 % of the variability and showed high RSME (~ 0.77), suggesting that other factors not considered here are important in regulating the magnitude of the bloom.

At BW, the SWLR model showed similar performance and coefficients to the one obtained for PV, i.e., $R^2 \sim 0.73$ and the same single relevant predictor, the negative Z_{eu}. The inverse relationship between the depth of the euphotic layer and the intensity of the bloom peak anomaly may be related to the attenuation of light by phytoplankton producing the shallowing of Z_{eu}. A study from a field cruise conducted in summer found that at the Burdwood Bank the water column was well mixed, hence light (as shown here), as well as the

action of heterotrophs seemed to regulate the bloom (Guinder et al., 2020). The RMSE ~ 0.55 and in several cases the match was not so good.

It is noteworthy that when the analysis was performed using the time series without first subtracting the weekly climatology, the resulting SWLR models included more predictors but explained a comparable (or slightly higher) proportion of the total variance. This highlights that removing the seasonal component enhances the statistical robustness of SWLR, as it avoids spurious correlations between the predictors and the dependent variable probably related to shared/similar seasonal variability.

4 Discussion

Phytoplankton bloom initiation has historically been framed through the lens of Sverdrup's (1953) critical depth hypothesis, where water column stratification enables phytoplankton to accumulate when the mixed layer shoals above a critical depth. This model was expanded by Siegel et al. (2002) and Taylor and Ferrari (2011), among others, to include turbulent mixing and intermittent stratification. While such models have effectively explained bloom phenology in large, open-ocean basins (e.g., North Atlantic, Henson et al., 2009, 2006), their application to complex shelf regions like the Argentine Shelf has remained limited. This region of the SWAO is rich in fisheries resources and relevant for CO_2 absorption (e.g., Angelescu and Prenski, 1987; Bianchi et al., 2009; Martinetto et al., 2019; Berghoff et al., 2023). Satellite information and models have predicted that phytoplankton blooms may be increasing in intensity and frequency in the overall area (Marrari et al., 2017; Dai et al., 2023). Nevertheless, the dynamics, and possible drivers, of phytoplankton growth is highly heterogeneous and still not studied enough in the region (e.g., Andreo et al., 2016; D2023).

Our findings reinforce the relevance of light-vertical mixing dynamics, quantified via the Z_{eu} : MLD ratio, in explaining the magnitude of blooms, but only in certain subregions. Unlike in the North Atlantic or Southern Ocean (Henson et al., 2009; Kauko et al., 2021), where clear seasonal water column stratification controls phenology, we observe that regions with strong tidal mixing or frontal activity, as well as the coastal site EP do not conform to these expectations. This kind of variability with upwelling/frontal or coastal systems driving blooms have been reported for other areas of world (Ferreira et al., 2021; Krug et al., 2018; Gittings et al., 2019; Kournopoulou et al., 2024).

This study brings to light the presence of distinct phenological regimes across the Argentine Shelf. In the Central Shelf (CS), we document bloom initiation as early as austral autumn or winter, i.e., months before stratification begins. These findings depart significantly from canonical models applied in temperate systems (Siegel et al., 2002; Racault et al., 2012) and may be related to recent observations of subseasonal bloom variability triggered by short-term increases in water column stability (Keerthi et al., 2021). This demonstrates the potential for intermittent water column stratification to facilitate early bloom formation, even when average conditions would suggest otherwise. A particular situation occurs on the coast of the CS, where blooms initiate and peak much earlier, probably due to the presence of phytoplankton species able to cope with turbidity vertical mixing, while still being exposed to some light due to the shallow bottom depth. It is worth mentioning that the Río de la Plata outflow exports to the continental shelf large amounts of water, nutrients, sediments, and carbon, which significantly influences the shelf's physical, chemical, and biological properties. This discharge creates a low-salinity plume that extends offshore ~ 600 km northwards and ~ 300 km southward, affecting sea surface temperature and vertical stratification. This must play an important role in controlling phytoplankton phenology, though its influence in the spatial climatology study was not specifically analyzed here since satellite-derived Chl-*a* is generally overestimated (Armstrong et al., 2004; Garcia et al., 2005, 2006) over the Río de La Plata plume due to high concentration of detritus (non-algal particles) and yellow substances (CDOM) content. Regarding the model study, only at the EP (EPEA) site the influence of the Río de la Plata waters has been previously reported on particular occasions in summer (Carreto et al., 1995), while the main bloom peak usually occurs in autumn-winter.

Further south, in the Patagonian Shelf (PS), bloom timing is more consistent with the Sverdrup framework, with peaks in spring and early summer. Yet even here, regions like the Patagonian shelf break exhibit complex behavior due to persistent nutrient input and local physical processes, similar to the Arctic and Bering Sea (Nielsen et al., 2024; Manizza et al., 2022), where phenology is shaped not only by stratification of the water column but also by ice dynamics and frontal zones. On the Patagonian shelf, frequent upwelling events bring nutrients to the surface, and frontal systems promote vertical mixing that disrupts the stable stratification, supporting intense surface phytoplankton blooms on the stratified side of the fronts and underscoring the region's high productivity of the Patagonian Shelf as a biological hotspot. These processes act primarily by enhancing nutrient availability and modulating light conditions in the surface layer, which is the focus of the present analysis based on satellite-derived surface chlorophyll-*a*. These findings are consistent with the conceptual frameworks of Sverdrup (1953) and Margalef (1978), who emphasized the roles of stratification and environmental variability in shaping ecosystem dynamics and phytoplankton strategies and ecosystem dynamics.

The spatial variation in B_{peak} across the study area highlights the critical role of water-column structure in modulating nutrient availability and light exposure, thereby determining bloom intensity. Bloom phenology in the Southwest Atlantic shows a complex spatial gradient modified by currents and fronts. The spatial distribution of the bloom tim-

Table 3. SWLR model performance (R^2 and RMSE) and predictor's coefficients at each site. Only coefficients statistically significant at the 95 % confidence level are shown.

	R^2	RMSE	PAR	Z_{eu}	Z_{eu4}	MLD	Z_{eu} : MLD	Z_{eu} : MLD_2	Z_{eu} : MLD_4	U-wind	U-$wind_2$
EP	0.72	0.554		−0.83						−0.27	
C4	0.75	0.523					−0.68		−0.329		
PV	0.73	0.532		−0.855							
SJ	0.92	0.314	0.242	−0.781					−0.471		−0.186
SS	0.87	0.390				−0.574	−0.913	−0.216			
BG	0.46	0.774			0.791			−1.251			
BW	0.73	0.534		−0.853							

ing phases found agree with a previous study, which focused only on the PS region of the SWAO (Andreo et al., 2016). The described patterns in this study emphasize the influence of regional oceanographic conditions on bloom dynamics across the Southwest Atlantic. Our study builds on these previous works in the Southwestern Atlantic (Andreo et al., 2016; D2023) that described regional patterns in chlorophyll concentration and bloom occurrence. However, those studies did not analyze bloom dynamics in terms of mechanistic controls, nor did they assess the regional validity of conceptual models such as euphotic and mixed layer depths. Here, by explicitly quantifying light and MLD, we show where traditional theory applies and where it fails.

When compared to global syntheses (Racault et al., 2012; Silva et al., 2021), our results underscore a key distinction: continental shelves feature sub-basin scale contrasts in phenology that are often obscured in basin-wide climatologies. This supports recent arguments that phenology metrics must be interpreted within their local physical and ecological contexts (Platt et al., 2005; Boyd and Doney, 2002).

This study echoes the view of Platt et al. (2009) and Kournopoulou et al. (2024) that phenology metrics such as bloom initiation, duration, and magnitude are powerful ecosystem indicators, but only when their regional drivers are understood. In regions like the Argentine Shelf, where physical drivers vary dramatically over small spatial scales, phenology must be framed within a region-specific, process-based context. For example, while Z_{eu} : MLD predicts anomalies in Bpeak well in parts of the Central and Northern Shelf, it fails in frontal or tidally mixed regions, indicating the need for hybrid approaches that integrate light, vertical mixing, nutrient input, and sub-seasonal variability (Keerthi et al., 2021; Henson et al., 2006).

Moreover, the study contributes to refining the phenoregion concept proposed by Krug et al. (2018), which classifies ocean regions based on the similarity of their seasonal phytoplankton dynamics and environmental forcing. Our findings confirm that the Argentine Shelf comprises multiple phenologically distinct regions (D2023), shaped not by latitude alone but by local oceanographic conditions. For instance, the Central Shelf supports early blooms probably driven by seasonal water column stratification subjected to intermittency; while in the Patagonian Shelf richer in nutrients due to its cold Sub-Antarctic waters as well as its several frontal areas, blooms develop later in summer being light their main driver. Even within each of these main regions (CS and PS) there are heterogeneities in the way that specific components of these two drivers (MLD and light) take prevalence in shaping the magnitudes of the blooms. Recognizing this mosaic of phenoregions is essential for capturing the spatial diversity of bloom behavior and improving ecological modeling, climate projections, and the design of targeted monitoring strategies.

Climate change is expected to increase water column stratification and alter wind and mixing regimes, thereby influencing bloom timing and community structure (Marinov et al., 2010; Boyd and Doney, 2002). In this regard, the northern section of the shelf (CS) may experience more intense stratifications, potentially favoring smaller phytoplankton and altering trophic pathways. Meanwhile, the southern region (PS) with higher nutrient input, would be more influenced by the stronger Westerly winds (Goyal et al., 2021; Deng et al., 2022) at the same time that cloudiness maybe increasing (Laken and Pallé, 2012); hence, whether phytoplankton would be really increasing in biomass, or just increasing its intracellular chlorophyll content is still a matter of speculation (Ryan-Keogh et al., 2023). Understanding how these subregions will respond differently is critical for modeling future productivity and for managing fisheries and ecosystem services in this economically important region.

5 Conclusions

The role of light availability, described by PAR and Z_{eu}, and MLD in shaping phytoplankton bloom dynamics across the SWAO shelf was analyzed. By examining satellite-derived Chl-*a* and environmental variables over a wide region, the study showed how these physical drivers influence bloom timing, intensity, and duration. The analysis addressed contrasting conditions at seven selected sites located in different phenological regions (according to D2023) that represented

a diversity of hydrographic regimes, revealing key details about site-specific phytoplankton phenology.

In the Central Shelf (CS), blooms typically initiate between May and August, with coastal regions experiencing even earlier initiation. These patterns were associated with shallow MLDs, which allowed sufficient light penetration to support early phytoplankton growth, probably associated with relatively stable atmospheric conditions. Conversely, the Patagonian Shelf (PS) exhibited delayed bloom initiation, generally occurring in September–November. This timing reflected the colder waters characteristic of the region, which required extended periods of warming to create MLD conditions favorable for phytoplankton growth. Additionally, nutrient-rich waters from Subantarctic origin and frontal systems supported high Chl-*a* during the austral summer, particularly near the shelf break. In such conditions, light penetration becomes a critical limiting factor for sustaining growth. These results indicate that light penetration, Z_{eu}, and its interplay with vertical mixing, Z_{eu} : MLD ratio, are key determinants of bloom phenology. Sverdrup's theory explains the general expected situation for the onset with phytoplankton growth favored when light penetration exceeds mixing depth ($Z_{eu} >$ MLD); we found here that in most cases at the time of the peak, though the Z_{eu} : MLD was around or higher than 1 (except for EP and BW), the strong phytoplankton growth would shallow Z_{eu}, and therefore negative Z_{eu} and Z_{eu} : MLD were good predictors of bloom peak anomaly. However, the predictive power of these correlations varied among the study sites. For instance, regions influenced by frontal zones or tidal mixing, such as the San Jorge Gulf and Grande Bay, exhibited more complex interactions, likely reflecting the additional contributions of localized nutrient fluxes or grazing pressure.

Seasonal cycles also showed clear mean spatial distribution patterns in bloom dynamics, with southern sites exhibiting longer bloom durations compared to northern regions. These findings emphasize the spatial heterogeneity of phytoplankton responses to environmental drivers, suggesting that while light and MLD are dominant factors, other local processes not considered here such as tidal energy, nutrient entrainment, and zooplankton grazing may significantly influence bloom phenology.

The study findings align with and complement those of D2023, who provided a broader regional perspective on the SWAO using 24 years of satellite-derived Chl-*a* data. D2023 classified the SWAO into nine biogeographical regions and documented significant long-term trends, including increased phytoplankton biomass and delayed autumn blooms. These trends were attributed to climate-driven warming, MLD shoaling, and extended stratification periods. In contrast, this study centered on understanding the mechanistic roles of light availability and MLD in driving bloom phenology at specific locations. While D2023 emphasized environmental changes, the present study explored finer-scale dynamics, providing information on how local variations in physical drivers shape bloom timing and intensity. Notably, this study confirmed D2023's observation of delayed bloom initiation in southern regions but added detail on the variability in bloom timing within individual subregions.

The results of the present study underscore the importance of physical factors, particularly light availability and MLD, in controlling bloom phenology. The observed spatial and temporal variability points to the need of localized analyses to capture the heterogeneity of phytoplankton responses to environmental changes. By integrating satellite observations with advanced statistical methods, the utility of regional-scale data in uncovering key agents of phytoplankton blooms is demonstrated.

Future research should incorporate additional data on nutrient fluxes, tidal energy, and zooplankton grazing to account for unexplained variability in bloom dynamics. Though here it was not attempted to disentangle physiological growth from ecological loss terms, this may be possible in a future if more observations allow a more robust modelling of net primary production. Secondary bloom dynamics and their ecological significance also warrant further investigation, particularly in the context of long-term trends (D2023). Finally, exploring the broader implications of climate-driven changes, including potential shifts in trophic interactions and ecosystem productivity, could provide useful clues into the resilience of these highly productive waters.

Data availability. The OC-CCI data can be downloaded from https://www.oceancolour.org/thredds/catalog/cci/v6.0-release/geographic/8day/chlor_a/catalog.html (last access: 22 July 2022), the Globcolour data from https://hermes.acri.fr/index.php?class=archive (last access: 30 July 2022), the GLORYS12v1 data from https://doi.org/10.48670/moi-00021 (CMEMS, 2025), and the ERA5 reanalysis data from https://doi.org/10.24381/cds.adbb2d47 (Hersbach et al., 2023). The results of this study, as well as the satellite and in-situ data used in producing the various figures, are available from the authors upon reasonable request.

Author contributions. AID, RAM, MLC, VAL, and RF jointly contributed to the conceptualization and design of the study. All authors participated equally in data analysis, interpretation of results, and drafting and revising the manuscript. AID and RAM prepared the figures including data processing, visualization, and layout. All authors reviewed and approved the final version of the manuscript.

Competing interests. The contact author has declared that none of the authors has any competing interests.

Disclaimer. Publisher's note: Copernicus Publications remains neutral with regard to jurisdictional claims made in the text, pub-

lished maps, institutional affiliations, or any other geographical representation in this paper. The authors bear the ultimate responsibility for providing appropriate place names. Views expressed in the text are those of the authors and do not necessarily reflect the views of the publisher.

Acknowledgements. The authors thank the Climate Change Initiative (CCI) Project, Globcolour and Coopernicus groups for the distribution of satellite merged products and modeled data. We acknowledge Instituto Nacional de Investigación y Desarrollo Pesquero (INIDEP) for the use of Z_{eu} data from the EPEA time series (DiPlaMCC program).

Financial support. This research has been supported by the Agencia Nacional de Promoción de la Investigación, el Desarrollo Tecnológico y la Innovación (grant no. PICT-2019 No. 2178). Robert Frouin was supported by the National Aeronautics and Space Administration (NASA) under grants 80NSSC19K1194 and 80NSSC24K13.

Review statement. This paper was edited by Liuqian Yu and reviewed by Emmanuel Boss and two anonymous referees.

References

Acha, E. M., Mianzan, H. W., Guerrero, R. A., Favero, M., and Bava, J.: Marine fronts at the continental shelves of austral South America: Physical and ecological processes, J. Mar. Syst., 44, 83–105, https://doi.org/10.1016/j.jmarsys.2003.09.005, 2004.

Acha, E. M., Ehrlich, M. D., Muelbert, J. H., Pájaro, M., Bruno, D., Machinandiarena, L., and Cadaveira, L.: Ichthyoplankton associated to the frontal regions of the southwestern atlantic, in: Plankton ecology of the southwestern Atlantic: From the subtropical to the subantarctic realm, edited by: Hoffmeyer M. S., Sabatini M. E., Brandini F. P., Calliari D. L., andSantinelli N. H., Berlin: Springer International Publishing, 219–246, https://doi.org/10.1007/978-3-319-77869-3_11, 2018.

Acha, E. M., Iribarne, O. O., and Piola, A. R.: The Patagonian Shelfbreak Front, Aquatic Ecology Series, 13, https://doi.org/10.1007/978-3-031-71190-9, 2024.

Aiken, L. S.: Multiple regression: Testing and interpreting interactions, Sage Publications, Inc., ISBN: 9780761907121, 1991.

Akselman, R.: Estudios ecológicos en el Golfo San Jorge y adyacencias (Atlántico Sudoccidental). Distribución, abundancia y variación estacional del fitoplancton en relación a factores físico-químicos y a la dinámica hidrográfica, PhD Thesis, Universidad de Buenos Aires, Argentina, 234 pp., https://bibliotecadigital.exactas.uba.ar/collection/tesis/document/tesis_n2857_Akselman (last access: 14 January 2026), 1996.

Andreo, V. C., Dogliotti, A. I., and Tauro, C. B.: Remote sensing of phytoplankton blooms in the Continental Shelf and shelf-break of Argentina: spatio-temporal changes and phenology, IEEE J. Sel. Top. Appl. Earth Obs. Remote Sens., 9, 5315–5324, https://doi.org/10.1109/JSTARS.2016.2585142, 2016.

Angelescu, V. and Prenski, L. B.: Ecología trófica de la Merluza común del Mar Argentino (Merlucciidae, Merluccius hubbsi). Parte 2. Dinámica de la alimentación analizada sobre la base de las condiciones ambientales, la estructura y las evaluaciones de los efectivos en su área de distribución, Serie Contribuciones del INIDEP 561, 1987.

Armstrong, R. A., Gilbes, F., Guerrero, R., Lasta, C., Benavidez, H., and Mianzan, H.: Validation of SeaWiFS-derived chlorophyll for the Rio de la Plata Estuary and adjacent waters, International Journal of Remote Sensing, 25, 1501–1505, 2004.

Begouen Demeaux, C., Boss, E., Graff, J. R., Behrenfeld, M. J., and Westberry, T. K.: Phytoplanktonic photoacclimation under clouds. Geophysical Research Letters, 52, e2024GL112274, https://doi.org/10.1029/2024GL112274, 2025.

Behrenfeld, M. J. and Falkowski, P. G.: Photosynthetic rates derived from satellite-based chlorophyll concentration, Limnol. Oceanogr., 42, 1–20, https://doi.org/10.4319/lo.1997.42.1.0001, 1997.

Behrenfeld, M. J., Boss, E., Siegel, D. A., and Shea, D. M.: Carbon-based ocean productivity and phytoplankton physiology from space, Global Biogeochem. Cycles, 19, https://doi.org/10.1029/2004GB002299, 2005.

Behrenfeld, M. J., O'Malley, R. T., Siegel, D. A., McClain, C. R., Sarmiento, J. L., Feldman, G. C., Milligan, A. J., Falkowski, P. G., Letelier, R. M., and Boss, E. S.: Climate-driven trends in contemporary ocean productivity, Nature, 444, 752–755, https://doi.org/10.1038/nature05317, 2006.

Berghoff, C. F., Pierrot, D. P., Epherra, L., Silva, R. I., Segura, V., Negri, R. M., Hozbor, M. C., Carignan, M. O., Barbero, L., and Lutz, V. A.: Physical and biological effects on the carbonate system during summer in the Northern Argentine Continental Shelf (Southwestern Atlantic), Journal of Marine Systems, 237, https://doi.org/10.1016/j.jmarsys.2022.103828, 2023.

Bertuche, D., Fischbach, C., Roux, A., Fernández, M., and Piñero, R.: Langostino (*Pleoticus muelleri*), in: Síntesis del estado de las Pesquerías Marítimas Argentinas y de la Cuenca del Plata. Años 1997–1998, con la actualización de 1999, edited by: Bezzi, S., Akselman, R., and Boschi, E. E., INIDEP, Mar del Plata, Argentina, 179–190, ISBN 987-96244-7-7-5, 2000.

Bianchi, A. A., Ruiz Pino, D., Isbert Perlender, H. G., Piola, A. R., Osiroff, A. P., Segura, V., Lutz, V., Luz Clara, M., and Balestrini, C. F.: Annual balance and seasonal variability of sea-air CO_2 fluxes in the Patagonian Sea: Their relationship with fronts and chlorophyll distribution, J. Geophys. Res., 114, C03018, https://doi.org/10.1029/2008JC004854, 2009.

Bogazzi, E., Baldoni, A., Rivas, A. L., Martos, P., Reta, R., Orensanz, J. M., Lasta, M., Arciprete, P., and Werner, F.: Spatial correspondence between areas of concentration of Patagonian Scallop (*Zygochlamys patagonica*) and frontal systems in the Southwestern Atlantic, Fish Oceanogr., 14, 359–376, https://doi.org/10.1111/j.1365-2419.2005.00340.x, 2005.

Boyd, P. W. and Doney, S. C.: Modeling regional responses by marine pelagic ecosystems to global climate change, Geophys. Res. Lett., 29, 1806, https://doi.org/10.1029/2001GL014130, 2002.

Carreto, J. I., Benavides, H. R., Negri, R. M., and Glorioso, P. D.: Toxic red-tide in the Argentine Sea. Phytoplankton distribution and survival of the toxic dinoflagellate *Gonyaulax excavate* in a frontal area, J. Plankton Res., 8, 15–28, https://doi.org/10.1093/plankt/8.1.15, 1986.

Carreto, J. I., Lutz, V. A., Carignan, M. O., Cucchi Colleoni, A. D., and De Marco, S. G.: Hydrography and chlorophyll a in a transect from the coast to the shelf-break in the Argentinian Sea, Cont. Shelf Res., 15, 315–336, https://doi.org/10.1016/0278-4343(94)E0001-3, 1995.

Carreto, J. I., Carignan, M. O., Montoya, N. G., and Cucchi Colleoni, A. D.: Ecología del fitoplancton en los sistemas frontales del Mar Argentino, in: El Mar Argentino y sus recursos pesqueros. Tomo 5, edited by: Carreto, J. I. and Bremec, C., El ecosistema marino, Publicaciones especiales del Instituto Nacional de Investigación y Desarrollo Pesquero, Mar del Plata 11–31, https://biblioteca.facimar.com.ar/cgi-bin/koha/opac-detail.pl?biblionumber=1185 (last access: 14 January 2026), 2007.

Carreto, J. I., Carignan, M. O., Montoya, N. G., Cozzolino, E., and Akselman, R.: Mycosporine-like amino acids and xanthophyll-cycle pigments favour a massive spring bloom development of the dinoflagellate Prorocentrum minimum in Grande Bay (Argentina), an ozone hole affected area, J. Mar. Syst., 178, 15–28, https://doi.org/10.1016/j.jmarsys.2017.10.004, 2018.

Cousseau, M. B. and Perrota, R. G.: Peces marinos de Argentina. Biología, distribución, pesca, Publicaciones Especiales INIDEP, Mar del Plata, 167 pp., ISBN 987-20245-4-5, 2004.

Cullen, J. J.: Diel vertical migration by dinoflagellates: roles of carbohydrate metabolism and behavioral flexibility, Contr. Mar. Sci., 27, 135–152, 1985.

Cullen, J.: Subsurface chlorophyll maximum layers: Enduring enigma or mystery solved?, Annu. Rev. Mar. Sci., 7, 207–239, https://doi.org/10.1146/annurev-marine-010213-135111, 2015.

Cushing, D. H.: A difference in structure between ecosystems in strongly stratified waters and in those that are only weakly stratified, J. Plankton Res., 11, 1–13, https://doi.org/10.1093/plankt/11.1.1, 1989.

Dai, Y., Yang, S., Zhao, D., Hu, C., Xu, W., Anderson, D. M., Li, Y., Song, X.-P., Boyce, D. G., Gibson, L., Zheng, C., and Feng, L.: Coastal phytoplankton blooms expand and intensify in the 21st century, Nature, 619, 603–609, https://doi.org/10.1038/s41586-023-05760-y, 2023.

Delgado, A. L., Hernaìndez-Carrasco, I., Combes, V., Font-MunÞoz, J., Pratolongo, P. D., and Basterretxea, G.: Patterns and trends in Chlorophyll-*a* concentration and phytoplankton phenology in the biogeographical regions of Southwestern Atlantic, J. Geophys. Res.: Oceans, 128, e2023JC019865, https://doi.org/10.1029/2023JC019865, 2023.

Deng, K., Azorin-Molina, C., Yang S., Hu, C., Zhang, G., Minola, L., and Chen, D.: Changes of Southern Hemisphere westerlies in the future warming climate, Atmos. Res., 270, 106040, https://doi.org/10.1016/j.atmosres.2022.106040, 2022.

Dogliotti, A. I., Lutz, V. A., and Segura, V.: Estimation of primary production in the southern Argentine continental shelf and shelf-break regions using field and remote sensing data, Rem. Sens. Environ., 140, 497–508, https://doi.org/10.1016/j.rse.2013.09.021, 2014.

E.U. Copernicus Marine Service Information (CMEMS): Global Ocean Physics Reanalysis, Marine Data Store (MDS) [data set], https://doi.org/10.48670/moi-00021, 2025.

Falkowski, P. G., Barber, R. T., and Smetacek, V.: Biogeochemical controls and feedbacks on ocean primary production, Science, 281, 200–206, https://doi.org/10.1126/science.281.5374.200, 1998.

Ferreira, A. S., Visser, A. W., MacKenzie, B. R., and Payne, M. R.: Accuracy and precision in the calculation of phenology metrics, J. Geophys. Res. Oceans, 119, 8438–8453, https://doi.org/10.1002/2014JC010323, 2014.

Ferreira, A., Brotas, V., Palma, C., Borges, C., and Brito, A. C.: Assessing Phytoplankton Bloom Phenology in Upwelling-Influenced Regions Using Ocean Color Remote Sensing, Remote Sens., 13, 675, https://doi.org/10.3390/rs13040675, 2021.

Forbes, M. C. and Garrafo, Z. A.: A note on the mean seasonal transport on the Argentinian Shelf, J. Geophys. Res., 93, 2311–2319, https://doi.org/10.1029/JC093iC03p02311, 1988.

Frouin, R., Franz, B. A., and Werdell, P. J.: The SeaWiFS PAR Product, in: Algorithm Updates for the Fourth SeaWiFS Data Reprocessing, NASA Tech. Memo. 2003-206892, edited by: Hooker, S. B. and Firestone, E. R., Greenbelt, Maryland: NASA Goddard Space Flight Center, Vol. 22, 46–50, 2003.

Garcia, C. A. E., Garcia, V. M. T., and McClain, C. R.: Evaluation of SeaWiFS chlorophyll algorithms in the Southwestern Atlantic and Southern Oceans, Remote Sensing of Environment, 95, 125–137, 2005.

Garcia, V. M. T., Signorini, S., Garcia, C. A. E., and McClain, C. R.: Empirical and semianalytical chlorophyll algorithms in the southwestern Atlantic coastal region (25–40° S and 60–45° W), International Journal of Remote Sensing, 27, 1539–1562, 2006.

Garzoli, S. L. and Garraffo, Z.: Transports, frontal motions and eddies at the Brazil-Malvinas currents confluence, Deep Sea Res. A.: Oceanogr. Res. Pap., 36, 1989, 681–703 https://doi.org/10.1016/0198-0149(89)90145-3, 1989.

Geider, R.: Light and temperature dependence of the carbon to chlorophyll a ratio in Microalgae and cyanobacteria: implications for physiology and growth of phytoplankton, New Phyto., 106, 1–34, 1987.

Giaccardi, M. and Caloni, N.: Frente Valdés: Línea de Base Ambiental y Socioeconómica. Documento del Ministerio de Ambiente y Desarrollo Sostenible, FAO y GEF. Proyecto "Fortalecimiento de la Gestión y Protección de la Biodiversidad Costero Marina en Áreas Ecológicas clave y la Aplicación del Enfoque Ecosistémico de la Pesca (EEP)" (Argentina), 185 pp., https://www.argentina.gob.ar/sites/default/files/2018/10/2022-1434_frentevaldes_0.pdf (last access: 14 January 2026), 2022.

Gittings, J. A., Raitsos, D. E., Kheireddine, M., Racault, M. F., Claustre, H., and Hoteit, I.: Evaluating tropical phytoplankton phenology metrics using contemporary tools, Sci. Rep., 9, 674, https://doi.org/10.1038/s41598-018-37370-4, 2019.

Glorioso, P. D.: Temperature distribution related to shelf-sea fronts on the Patagonian Shelf, Cont. Shelf Res., 7, 27–34, https://doi.org/10.1016/0278-4343(87)90061-6, 1987.

Glorioso, P. D. and Flather, R. A.: The Patagonian Shelf tides, Prog. Oceanogr., 40, 263–283, https://doi.org/10.1016/S0079-6611(98)00004-4, 1997.

González-Reyes, A., Christie, D. A., Schneider-Valenzuela, I., Venegas-González, A., Muñoz, A. A., Hadad, M., Gipoulou-Zuñiga, T., Tapia-Marzan, V., Gibson-Carpintero, S., and Santini-Junior, L.: Recent multispecies tree-growth decline reveals a severe aridity change in Mediterranean Chile, En-

viron. Res. Lett., 19, 064046, https://doi.org/10.1088/1748-9326/ad4049, 2024.

Goyal, R., Gupta, A. S., Jucker, M., and England, M. H.: Historical and projected changes in the Southern Hemisphere Surface westerlies, Geophys. Res. Lett., 48, https://doi.org/10.1029/2020GL090849, 2021.

Guerrero, R. A. and Piola, A. R.: Masas de agua en la plataforma continental. En: El Mar Argentino y sus recursos pesqueros. Antecedentes históricos de las exploraciones en el mar y las características ambientales,Vol. 1, Ed: E. E. Boschi, Instituto Nacional de Investigaciones y Desarrollo Pesquero, Mar del Plata, Argentina, 107–118, https://aquadocs.org/items/93fea682-70b2-4775-9a8e-649b5ff3a72c (last access: 14 January 2026), 1997.

Guinder, V. A., Malits A., Ferronato C., Krock B., Garzón-Cardona J., and Martínez A.: Microbial plankton configuration in the epipelagic realm from the Beagle Channel to the Burdwood Bank, a Marine Protected Area in Sub-Antarctic waters, PLoS ONE, 15, e0233156, https://doi.org/10.1371/journal.pone.0233156, 2020.

Henson, S. A., Robinson, I., Allen, J. T., and Waniek, J. J.: Effect of meteorological conditions on interannual variability in timing and magnitude of the spring bloom in the Irminger Basin, North Atlantic, Deep-Sea Res. Part I, 53, 1601–1615, https://doi.org/10.1016/j.dsr.2006.07.009, 2006.

Henson, S. A., Dunne, J. P., and Sarmiento, J. L.: Decadal variability in North Atlantic phytoplankton blooms, J. Geophys. Res. Oceans, 114, https://doi.org/10.1029/2008JC005139, 2009.

Hersbach, H., Bell, B., Berrisford, P., Biavati, G., Horányi, A., Muñoz Sabater, J., Nicolas, J., Peubey, C., Radu, R., Rozum, I., Schepers, D., Simmons, A., Soci, C., Dee, D., and Thépaut, J.-N.: ERA5 hourly data on single levels from 1940 to present, Copernicus Climate Change Service (C3S) Climate Data Store (CDS) [data set], https://doi.org/10.24381/cds.adbb2d47, 2023.

Höflich, O.: Climate of the South Atlantic, in: Climate of the oceans, edited by: Van Loon, H., Elsevier, Amsterdam, 1–191, ISBN 0444413375, 1984.

Kauko, H. M., Hattermann, T., Ryan-Keogh, T., Singh, A., de Steur, L., Fransson, A., Chierici, M., Falkenhaug, T., Hallfredsson, E. H., Bratbak, G., Tsagaraki, T., Berge, T., Zhou, Q., and Moreau, S.: Phenology and environmental control of phytoplankton blooms in the Kong Håkon VII Hav in the Southern Ocean, Front. Mar. Sci., 8, 623856, https://doi.org/10.3389/fmars.2021.623856, 2021.

Keerthi, M. G., Lévy, M., and Aumont, O.: Intermittency in phytoplankton bloom triggered by modulations in vertical stability, Sci. Rep., 11, 1133, https://doi.org/10.1038/s41598-020-80331-z, 2021.

Kournopoulou, A., Kikaki, K., Varkitzi, I., Psarra, S., Assimakopoulou, G., Karantzalos, K., and Raitsos, D. E.: Atlas of phytoplankton phenology indices in selected Eastern Mediterranean marine ecosystems, Sci. Rep., 14, 1236, https://doi.org/10.1038/s41598-024-60792-2, 2024.

Krug, L. A., Platt, T., Sathyendranath, S., and Barbosa, A. B.: Patterns and drivers of phytoplankton phenology off SW Iberia: a phenoregion based perspective, Prog. Oceanogr., 165, 233–256, https://doi.org/10.1016/j.pocean.2018.06.010, 2018.

Laken, B. A. and Pallé, E.: 2012: Understanding sudden changes in cloud amount: The Southern Annular Mode and South American weather fluctuations, J. Geophys. Res., 117, D13103, https://doi.org/10.1029/2012JD017626, 2012.

Lellouche, J.-M., Grenier, E., Bourdalle-Badie, R., Garric, G., Angelique, M., Marie, D., Clément, B., Hamon, M.L, Le Galloudec, O., Regnier C., Candela, T., Testut, C.-E., Gasparin, F., Ruggiero G., Benkiran, M., Drillet, Y., and Le Traon, P.-Y.: The Copernicus global 1/12 degree oceanic and sea ice GLORYS12 reanalysis, Front. Earth Sci., 9, 698876, https://doi.org/10.3389/feart.2021.698876, 2021.

Li, Y., Li, J., Zhao, Y., Lei, M., Zhao, Y., Jian, B., Zhang, M., and Huang, J.: Long-term variation of boundary layer height and possible contribution factors: A global analysis, Sci. Total Environ., 796, 148950, https://doi.org/10.1016/j.scitotenv.2021.148950, 2021.

Lucas, A. J., Guerrero, R. A., Mianzan, H. W., Acha, E. M., and Lasta, C. A.: Coastal oceanographic regimes of the Northern Argentine Continental Shelf (34–43° S), Estuar. Coast. Shelf Sci., 65, 405–420, https://doi.org/10.1016/j.ecss.2005.06.015, 2005.

Lutz, V. A. and Carreto, J. I.: A new spectrofluorometric method for the determination of chlorophylls and degradation products and its application in two frontal areas of the Argentine Sea, Cont. Shelf Res., 11, 433–451, https://doi.org/10.1016/0278-4343(91)90052-8, 1991.

Lutz, V. A., Subramaniam, A., Negri, R. M., Silva, R. I., and Carreto, J. I.: Annual variations in bio-optical properties at the "Estación Permanente de Estudios Ambientales (EPEA)" coastal station, Argentina, Cont. Shelf Res., 26, 1093–1112, https://doi.org/10.1016/j.csr.2006.02.012, 2006.

Lutz, V. A., Segura, V., Dogliotti, A. I., Gagliardini, D. A. Bianchi, A. A., and Balestrini, C. F.: Primary production in the Argentine Sea during spring estimated by field and satellite models, Journal of Plankton Research, 32, 181–195, https://doi.org/10.1093/plankt/fbp117, 2010.

Luz Clara, M.: Estimación de los flujos mar-atmósfera de CO_2 y la variabilidad de la clorofila-a en el Mar Argentino. Lic. en Oceanografía, Bch. Thesis, Facultad de Ciencias Exactas y Naturales, Universidad de Buenos Aires, Argentina, https://aquadocs.org/items/03aee2b1-4308-461d-a170-9852222d9393 (last access: 14 January 2026), 2008.

Luz Clara, M., Simionato, C. G., D'Onofrio, E., Fiore, M., and Moreira, D.: Variability of tidal constants in the Río de la Plata estuary associated to the natural cycles of the runoff, Estuar. Coast. Shelf Sci., 148, 85–96, https://doi.org/10.1016/j.ecss.2014.07.002, 2014.

Luz Clara, M., Simionato, C. G., D'Onofrio, E., and Moreira, D.: Future sea level rise and changes on tides in the Patagonian Continental Shelf, J. Coast. Res., 31, 519–535, https://doi.org/10.2112/JCOASTRES-D-13-00127.1, 2015.

Manizza, M., Carroll, D., and Menemenlis, D.: Modeling the recent changes of phytoplankton blooms dynamics in the Arctic Ocean, J. Geophys. Res. Oceans, 127, e2022JC019152, https://doi.org/10.1029/2022JC019152, 2022.

Marchese, C., Albouy, C., Tremblay, JÉ., Dumont, D., D'Ortenzio, F., Vissault, S., and Bélanger, S.: Changes in phytoplankton bloom phenology over the North Water (NOW) polynya: a response to changing environmental conditions, Polar Biol., 40, 1721–1737, https://doi.org/10.1007/s00300-017-2095-2, 2017.

Margalef, R.: Life-forms of phytoplankton as survival alternatives in an unstable environment, Oceanol. Acta, 1, 493–509, 1978.

Marinov, I., Doney, S. C., and Lima, I. D.: Response of ocean phytoplankton community structure to climate change over the 21st century: partitioning the effects of nutrients, temperature and light, Biogeosciences, 7, 3941–3959, https://doi.org/10.5194/bg-7-3941-2010, 2010.

Marrari, M., Piola, A. R., and Valla, D.: Variability and 20-year trends in satellite-derived surface chlorophyll concentrations in large marine ecosystems around South and Western Central America, Front. in Mar. Sci., 4, https://doi.org/10.3389/fmars.2017.00372, 2017.

Martín de Nascimento, J., Schloss, I., Malits, A., Flores Melo, X., Iachetti , C., Latorre, M., Alder, V. A., Bértola, G., Olguin Salinas, H., Capitanio, F. L., and Spinelli, M. L.: El Banco Burdwood: Un oasis sumergido en el Atlántico Sur, La Lupa, Colección Fueguina De divulgación científica, 10–13, http://hdl.handle.net/11336/213883 (last access: 16 January 2026), 2020.

Martinetto, P. M. R, Alemany, D., Botto, F., Mastrángelo, M., Falabella, V., Acha, E. M., Antón, G., Bianchi, A., Campagna, C., Cañete, G., Filippo, P., Iribarne, O. O., Laterra, P., Martínez, P., Negri, R., Piola, A. R., Romero, S. I., Santos, D., and Saraceno, M.: Linking the scientific knowledge on marine frontal systems with ecosystem services, Ambio, 49, 541–556, https://doi.org/10.1007/s13280-019-01222-w, 2019.

Martos, P. and Piccolo, M. C.: Hydrography of the Argentine Continental Shelf between 38° S and 42° S, Cont. Shelf Res., 8, 1043–1056, https://doi.org/10.1016/0278-4343(88)90038-6, 1988.

Matano, R. P., Palma, E. D., and Piola, A. R.: The influence of the Brazil and Malvinas Currents on the Southwestern Atlantic Shelf circulation, Ocean Sci., 6, 983–995, https://doi.org/10.5194/os-6-983-2010, 2010.

Moore, C. M., Mills, M. M., Arrigo, K. R., Berman-Frank, I., Bopp, L., Boyd, P. W., Galbraith, E. D., Geider, R. J., Guieu, C., Jaccard, S. L., Jickells, T. D., La Roche, J., Lenton, T. M., Mahowald, N. M., Marañón, E., Marinov, I., Moore, J. K., Nakatsuka, T., Oschlies, A., Saito, M. A., Thingstad, T. F., Tsuda, A., and Ulloa, O.: Processes and patterns of oceanic nutrient limitation, Nature Geosci., 6, 701–710, https://doi.org/10.1038/ngeo1765, 2013.

Moreira, D., Simionato, C. G., and Dragani, W.: Modeling ocean tides and their energetics in the North Patagonia Gulfs of Argentina, J. Coast. Res., 27, 87–102, https://doi.org/10.2112/JCOASTRES-D-09-00055.1, 2011.

Morel, A., Huot, Y., Gentili, B., Werdell, P. J., Hooker, S. B., and Franz, B.A.: Examining the consistency of products derived from various ocean color sensors in open ocean (case 1) waters in the perspective of a multi-sensor approach, Rem. Sens. Environ., 111, 69–88, https://doi.org/10.1016/j.rse.2007.03.012, 2007.

Moriondo Danovaro, P., Fernández, M., Fischbach, C., de la Garza, J., and Bertuche D.: Síntesis de los aspectos biológico-pesqueros del langostino (Pleoticus muelleri, Decapoda, Solenoceridae), in: El mar Argentino y sus recursos pesqueros, edited by: Boschi, E. E., Tomo 6, INIDEP, Mar del Plata, 95–110, ISBN 978-987-1443-11-6, 2016.

Nielsen, J. M., Sigler, M. F., Eisner, L. B., Watson, J. T., Rogers, L. A., Bell, S. W., Pelland, N., Mordy, C. W., Cheng, W., Kivva, K., Osborne, S., and Stabeno, P.: Spring phytoplankton bloom phenology during recent climate warming on the Bering Sea shelf, Progr. Oceanogr., 214, 103176, https://doi.org/10.1016/j.pocean.2023.103176, 2024.

Piola, A. R. and Matano, R. P.: The South Atlantic Western Boundary Currents Brazil/Falkland (Malvinas) Currents, Encyclopedia of Ocean Sciences, edited by: Steele, J. M., Thorpe, S. A., and Turekian, K. K., Academic Press, 1, 340–349, ISBN 012227430X, 2001.

Piola, A. R., Palma, E. D., Bianchi, A. A., Castro, B. M., Dottori, M., Guerrero, R. A., Marrari, M., Matano, R. P., Möller Jr., O. O., and Saraceno, M.: Physical oceanography of the SW Atlantic shelf: A review, in: Plankton Ecology of the Southwestern Atlantic, edited by: Hoffmeyer, M., Sabatini, M., Brandini, F., Calliari, D., and Santinelli, N., Springer Nature, https://doi.org/10.1007/978-3-319-77869-3, 2018.

Platt, T.: Primary production of the ocean water column as a function of surface light intensity: Algorithms for remote sensing, Deep Sea Res. A: Oceanogr. Res. Pap., 33, 149–163, https://doi.org/10.1016/0198-0149(86)90115-9, 1986.

Platt, T. and Sathyendranath, S.: Ecological indicators for the pelagic zone of the ocean from remote sensing, Rem. Sens. Environ., 112, 3426–3436, https://doi.org/10.1016/j.rse.2007.10.016, 2008.

Platt, T., Bouman, H., Devred, E., Fuentes-Yaco, C., and Sathyendranath, S.: Physical forcing and phytoplankton distributions, Sci. Mar., 69, 55–73, https://doi.org/10.3989/scimar.2005.69s155, 2005.

Platt, T., White III, G. N., Zhai, L., Sathyendranath, S., and Roy, S.: The phenology of phytoplankton blooms: Ecosystem indicators from remote sensing, Ecol. Model., 221, 1574–1587, https://doi.org/10.1016/j.ecolmodel.2008.11.022, 2009.

Racault, M.-F., Le Quere, C., Buitenhuis, E., Sathyendranath, S., and Platt, T.: Phytoplankton phenology in the global ocean, Ecol. Indic., 14, 152–163, https://doi.org/10.1016/j.ecolind.2011.07.010, 2012.

Racault, M., Sathyendranath, S., and Platt, T.: Impact of missing data on the estimation of ecological indicators from satellite ocean-colour time-series, Rem. Sens. Environ., 152, 15–28, https://doi.org/10.1016/j.rse.2014.05.016, 2014.

Richardson, K. and Bendtsen, J.: Vertical distribution of phytoplankton and primary production in relation to nutricline depth in the open ocean, Mar. Ecol. Prog. Ser., 620, 33–46, https://doi.org/10.3354/meps12960, 2019.

Rivas, A. L. and Pisoni, J. P.: Identification, characteristics and seasonal evolution of surface thermal fronts in the Argentinean Continental Shelf, J. Mar. Syst., 79, 134–143, https://doi.org/10.1016/j.jmarsys.2009.07.008, 2010.

Ruiz, M. G., Lutz, V., Segura, V., Berghoff, C., and Negri, R.: The color of EPEA: Variability in the bio-optical properties in the period 2000–2017, Mar. Fish. Sci., 33, 205–225, https://doi.org/10.47193/mafis.3322020301105, 2020.

Ruiz-Etcheverry, L. A., Saraceno, M., Piola, A. R., and Strub, P. T.: Sea level anomaly on the Patagonian continental shelf: trends, annual patterns and geostrophic flows, J. Geophys. Res. Oceans, 121, 2733–2754, https://doi.org/10.1002/2015JC011265, 2016.

Ryan-Keogh, T. J., Thomalla, S. J., Monteiro, P. M. S., and Tagliabue, A.: Multidecadal trend of increasing iron stress in Southern Ocean phytoplankton, Science, 379, 834–840, 2023.

Sabatini, M. and Martos, P.: Mesozooplankton features in a frontal area off northern Patagonia (Argentina) during spring 1995 and 1998, Sci. Mar., 66, 215–232, https://doi.org/10.3989/scimar.2002.66n3215, 2002.

Sabatini, M., Reta, R., and Matano, R.: Circulation and zooplankton biomass distribution over the southern Patagonian shelf during late summer, Cont. Shelf Res., 24, 1359–1373, https://doi.org/10.1016/j.csr.2004.03.014, 2004.

Sathyendranath, S., Stuart, V., Nair, A., Oka, K., Nakane, T., Bouman, H., Forget, M.H., Maass, H., and Platt, T.: Carbon-to-chlorophyll ratio and growth rate of phytoplankton at the sea, Mar. Ecol. Prog. Ser., 383, 73–84, https://doi.org/10.3354/meps07998, 2009.

Sathyendranath, S., Brewin, R. J., Brockmann, C., Brotas, V., Calton, B., Chuprin, A., Cipollini, P., Couto, A. B., Dingle, J., Doerffer, R., Donlon, C., Dowell, M., Farman, A., Grant, M., Groom, S., Horseman, A., Jackson, T., Krasemann, H., Lavender, S., Martinez-Vicente, V., Mazeran, C., Mélin, F., Moore, T. S., Müller, D., Regner, P., Roy, S., Steele, C. J., Steinmetz, F., Swinton, J., Taberner, M., Thompson, A., Valente, A., Zühlke, M., Brando, V. E., Feng, H., Feldman, G., Franz, B. A., Frouin, R., Gould, R. W. Jr., Hooker, S. B., Kahru, M., Kratzer, S., Mitchell, B.G., Muller-Karger, F. E., Sosik, H. M., Voss, K. J., Werdell, J., and Platt, T.: An ocean-colour time series for use in climate studies: the experience of the ocean-colour climate change initiative (OC-CCI), Sensors, 19, 4285, https://doi.org/10.3390/s19194285, 2019.

Segura, V., Lutz, V. A., Dogliotti, A. I., Silva, R., Negri, R., Akselman, R., and Benavides, H.: Phytoplankton Functional Types and primary production in the Argentine Sea, Mar. Ecol. Prog. Ser., 491, 15–31, https://doi.org/10.3354/meps10461, 2013.

Segura, V., Silva, R., Luz Clara, M., Martos, P., Cozzolino, E., and Lutz, V.: Primary production and plankton assemblages in the fisheries ground around San Jorge Gulf (Patagonia), Plankton Benthos Res., 16, 24–39, https://doi.org/10.3800/pbr.16.24, 2021.

Siegel, D. A., Doney, S. C., and Yoder, J. A.: The North Atlantic Spring Phytoplankton Bloom and Sverdrup's Critical Depth Hypothesis, Science, 296, 730–733, https://doi.org/10.1126/science.1069174, 2002.

Silva, E., Counillon, F., Brajard, J., Korosov, A., Pettersson, L. H., Samuelsen, A., and Keenlyside, N.: Twenty-one years of phytoplankton bloom phenology in the Barents, Norwegian, and North Seas, Front. Mar. Sci., 8, 746327, https://doi.org/10.3389/fmars.2021.746327, 2021.

Silva, R. I., Negri, R. M., and Lutz, V.: Summer succession of ultraphytoplankton at the EPEA coastal station (Northern Argentina), J. Plankton Res., 31, 447–458, https://doi.org/10.1093/plankt/fbn128, 2009.

Strub, P. T., James, C., Combes, V., Matano, R. P., Piola, A. R., Palma, E. D., Saraceno, M., Guerrero, R. A., Fenco, H., and Ruiz-Etcheverry, L. A.: Altimeter-derived seasonal circulation on the southwest Atlantic shelf: 27°–43° S, J. Geophys. Res. Oceans, 120, https://doi.org/10.1002/2015JC010769, 2015.

Sverdrup, H. U.: On conditions for the vernal blooming of phytoplankton, Journal du Conseil, 18, 287–295, 1953.

Taylor, J. R. and Ferrari, R.: Shutdown of turbulent convection as a new criterion for the onset of spring phytoplankton blooms, Limnol. Oceanogr., 56, 2293–2307, https://doi.org/10.4319/lo.2011.56.6.2293, 2011.

Torres, F. L. R., Kuki, C. A. C, Reboita, M. S., Lima, L. M. M., Lima, J. W. M., and de Queiroz, A. R.: Refining Seasonal Precipitation Forecast in Brazil Using Simple Data-Driven Techniques and Climate Indices, Revista Brasileira de Meteorologia, 39, e39240052, https://www.scielo.br/j/rbmet/a/HdvhCqgXTjCNsqTwSxRHpXL/?format=html&lang=en (last access: 10 February 2026), 2024.

Trenberth, K. E.: Storm tracks in the Southern Hemisphere, J. Atmos. Sci., 48, 2159–2178, https://doi.org/10.1175/1520-0469(1991)048<2159:STITSH>2.0.CO;2, 1991.

Valente, A., Sathyendranath, S., Brotas, V., Groom, S., Grant, M., Taberner, M., Antoine, D., Arnone, R., Balch, W. M., Barker, K., Barlow, R., Bélanger, S., Berthon, J.-F., Beşiktepe, Ş., Borsheim, Y., Bracher, A., Brando, V., Canuti, E., Chavez, F., Cianca, A., Claustre, H., Clementson, L., Crout, R., Frouin, R., García-Soto, C., Gibb, S. W., Gould, R., Hooker, S. B., Kahru, M., Kampel, M., Klein, H., Kratzer, S., Kudela, R., Ledesma, J., Loisel, H., Matrai, P., McKee, D., Mitchell, B. G., Moisan, T., Muller-Karger, F., O'Dowd, L., Ondrusek, M., Platt, T., Poulton, A. J., Repecaud, M., Schroeder, T., Smyth, T., Smythe-Wright, D., Sosik, H. M., Twardowski, M., Vellucci, V., Voss, K., Werdell, J., Wernand, M., Wright, S., and Zibordi, G.: A compilation of global bio-optical in situ data for ocean-colour satellite applications – version two, Earth Syst. Sci. Data, 11, 1037–1068, https://doi.org/10.5194/essd-11-1037-2019, 2019.

Vera, C. S., Vigliarolo, P. K., and Berbery, E. H.: Cold season synoptic-scale waves over subtropical South America, Mon. Weather Rev., 2, https://doi.org/10.1175/1520-0493(2002)130<0684:CSSSWO>2.0.CO;2, 2002.

Yang, C., Wang, N., and Wang, S.: A comparison of three predictor selection methods for statistical downscaling, Int. J. Climatol., 37, 1238–1249, https://doi.org/10.1002/joc.4772, 2017.

Yu, S., Bai, Y., He, X., Li, T., and Gong, F.: A new merged dataset of global ocean chlorophyll-*a* concentration for better trend detection, Front. Mar. Sci., 10, 48, https://doi.org/10.3389/fmars.2023.1051619, 2023.

Zhao, H., Matsuoka, A., Manizza, M., and Winter, A.: Recent changes of phytoplankton bloom phenology in the northern high-latitude oceans (2003–2020), Journal of Geophysical Research: Oceans, 127, e2021JC018346, https://doi.org/10.1029/2021JC018346, 2022.